FERMILAB-PUB-07-315-T

FERMILAB-PUB-07-315-T
BNL-HET-07/10

arXiv:0707.0212v1 [hep-ph] 1 Jul 2007

Footprints of the Beyond in flavor physics: Possible role of the Top Two Higgs Doublet Model

Enrico Lunghi[1] and Amarjit Soni[2]

[1] *Fermi National Accelerator Laboratory*
P.O. Box 500 , Batavia, IL, 60510-0500, USA
E-mail: lunghi@fnal.gov

[2] *Physics Department, Brookhaven National Laboratory,*
Upton, New York, 11973, USA
E-mail: soni@quark.phy.bnl.gov

Abstract

The B-factories results provide an impressive confirmation of the Standard Model (SM) description of flavor and CP violation. Nevertheless, as more data were accumulated, deviations in the 2.5-3.5 σ range have emerged pointing to the exciting possibility of new CP-odd phase(s) and flavor violating parameters in B-decays. Primarily this seems to be the case in the time dependent CP asymmetries in penguin dominated modes (e.g. $B \to \phi(\eta')K_s$). We discuss these and other deviations from the SM and, as an illustration of possible new physics scenarios, we examine the role of the Top Two Higgs Doublet Model. This is a simple extension of the SM obtained by adding second Higgs doublet in which the Yukawa interactions of the two Higgs doublets are assigned in order to naturally account for the large top-quark mass. Of course, many other extensions of the Standard Model could also account for these experimental deviations. Clearly if one takes these deviations seriously then some new particles in the $\approx$ 300 GeV to $\approx$ few TeV with associated new CP-odd phase(s) are needed.

1 Introduction

The spectacular performance of the two asymmetric B-factories is a triumph of accelerator science. Both machines appreciably exceeded their designed luminosities and presently have delivered over 1 ab^{-1} of data [1].

On the one hand, the first crucial result is a striking confirmation of CKM–paradigm [2] of flavor and CP violation. It is clear that the CKM phase provides the dominant explanation for the observed CP violation to an accuracy of about 10-15%. This strongly suggests that new physics most likely can only show up as a perturbation requiring accurate measurements and precise theoretical calculations.

On the other hand, many B-factory results indicate interesting deviations from the SM. One of the most compelling hints of new physics are the measurements of the time-dependent CP asymmetries in penguin dominated modes that turned out to be systematically smaller than the SM expectation. While the calculation of these asymmetries requires to keep under control long distance QCD effects, the QCD factorization as well as several other approaches shows that some of the modes are extremely clean (*i.e.* ϕK_s, $\eta' K_s$ and $K_s\ K_s\ K_s$ final states). The magnitude of the deviation ranges from 2.5σ to about 4σ depending on how one chooses to compare. The amplitudes for these decays are dominated by penguin (*i.e.* short distance) contributions: hence, deviations in these CP asymmetries are expected and quite natural in a very wide class of new physics scenarios. It is therefore extremely important to follow this issue very closely.

Unfortunately a sizable reduction of the experimental errors on these asymmetries requires significantly greater statistics and is bound to be slow: the projected doubling of the integrated luminosity by the end of 2008 is unlikely to resolve this issue in a decisive fashion. From a theoretical point of view, it would be extremely desirable to reduce the experimental uncertainties at the 5% level because a Standard Model irreducible pollution of a few percents is expected. The needed luminosity for this important enterprise may have to await the advent of a Super-B factory [3–5].

In addition to this hint for new physics there are several other measurements that deviate sizably from the respective SM expectations. Among those we have the muon anomalous magnetic moment, difference in direct CP asymmetries in $B \to K\pi$ decays and the tension between $|V_{ub}|$ and the time-dependent CP asymmetry in $B \to J/\psi K_s$. In this paper, we present an extensive discussion of several important experimental hints for deviations from the SM. As an illustration we study how a simple and well motivated extension of the SM (the Top Two Higgs Doublet Model [6–8]) can handle the experimental data.

Needless to say, the deviations seen in B decays [9] and some other aspects of flavor physics, may also be accountable by many other extensions of the SM; for example supersymmetry [10], a fourth family [11], a Z-penguin [12], warped flavor-dynamics [13] etc. Clearly, the key features of any beyond the Standard Model scenario that is to account for the experimental deviations in B-physics and other flavor physics that are being discussed here are that it has to have at least one new CP-odd phase and new particles in the ≈ 300 GeV to $\approx$ few TeV range. Much more experimental information is required to disentangle the various possibilities.

In Sec. 2 we present the list of problematic measurements that we consider and summarize them in a *pull* table. In Sec. 3 we give a short overview of the Top Two Higgs Doublet Model (T2HDM). In Sec. 4 we perform a chi-squared analysis of the T2HDM and show how present experimental results, using observables that are relatively clean, constrain its parameter space. In Secs. 5 and 6 we present details of the calculation of T2HDM contributions to various observables. A brief summary and outlook is given in Sec. 7.

2 Possible hints for deviations from the SM

In this section we summarize some of the experimental problems that have surfaced in the past few years connected with the Standard Model picture of flavor physics. In particular we focus on the tension between the measured time dependent CP asymmetry in $B \to J/\psi K_s$ and the rest of the unitarity triangle fit, the discrepancy between CP asymmetries in $b \to s\bar{s}s$ (*e.g.* $B \to (\phi, \eta')K_s$) and $b \to c\bar{c}s$ ($B \to J/\psi K_s$) transitions, the difficulties in describing the CP asymmetries in the decays $B^0 \to K^+\pi^-$ and $B^- \to K^-\pi^0$, the anomalous magnetic moment of the muon and the forward-backward asymmetry in $Z \to b\bar{b}$.

$a_{\psi K}$: Standard Model prediction vs direct measurement

The standard unitarity triangle fit, with the inclusion of the constraints from $|V_{ub}/V_{cb}|$, ε_K, ΔM_{B_s} and ΔM_{B_d} predicts $a_{\psi K} = \sin(2\beta) = 0.78 \pm 0.04$. Here, we used a simple χ^2 fit in which we use the inputs given in Table 1 and assume that all errors are gaussian (this means, for instance, that we combine systematic and statistical errors in quadrature). The direct determination of this asymmetry via the "gold - plated" ψK_s modes "yields [14] $a_{\psi K}^{WA} = 0.675 \pm 0.026$ and deviates from the SM prediction by about two standard deviations. In Fig. 1 we show the SM fit of the unitarity triangle in the $(\bar{\rho}, \bar{\eta})$ plane and the $a_{\psi K}$ constraint is superimposed. From the figure it is clear that this effect is mainly due to the conflict between $a_{\psi K}$ and $|V_{ub}|$. Note also that the former measurement is clean from hadronic uncertainties and the latter uses basically a tree–level process.

In order to test the stability of this 2σ effect, it is useful to entertain a scenario in which the errors on $|V_{ub}/V_{cb}|$ and on the SU(3) breaking ratio obtained by lattice calculations ξ_s are increased. Increasing $\delta|V_{ub}/V_{cb}| = 10\%$ (from about 7%) and $\delta\xi_s = 0.06$ (from 3-4%), the prediction for $sin2\beta$ does not change much: we find $\sin(2\beta) = 0.78 \pm 0.05$. It is also interesting to consider the impact of the very recent lattice determination of $\hat{B}_K$ presented in Ref. [15]: using $\hat{B}_K = 0.765 \pm 0.017 \pm 0.040$, the fit gets slightly worse and the prediction for $\sin 2\beta$ reads 0.76 ± 0.035. The conclusion of these exercises is that the strain between the direct determination of $a_{\psi K}$ and the rest of the unitarity triangle fit is quite solid [16].

Time–dependent CP asymmetries in $b \to s\bar{s}s$ modes

Within the SM, the CP asymmetries in penguin dominated $b \to s$ transitions such as ϕK_s and $\eta' K_s$ are equal to $\sin(2\beta)$ up to penguin polluting effects, that are expected to be fairly small in

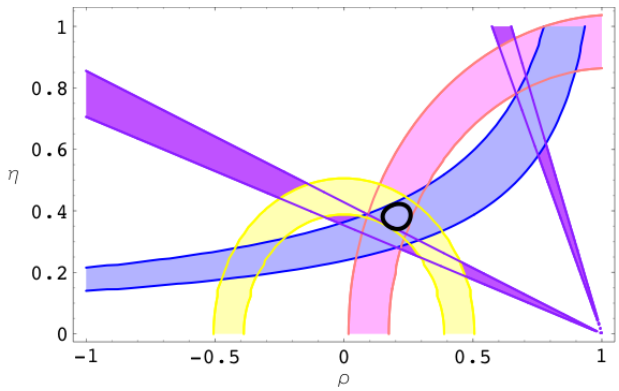

Figure 1: Unitarity triangle fit in the SM. The constraints from $|V_{ub}/V_{cb}|$, ε_K, $\Delta M_{B_s}/\Delta M_{B_d}$ are included in the fit; the region allowed by $a_{\psi K}$ is superimposed.

these modes [17–19]. The calculation of matrix elements of penguin operators is an intrinsically non–perturbative task, and it has been recently studied using many different approaches [20–23]. These studies show that while a precise calculation of hadronic uncertainties is very difficult, at least three cases, namely $\eta' K_s$, ϕK_s and $K_s K_s K_s$ [24] are notably clean with only a few percent contaminations. In many other cases rough estimates (see for instance Refs. [19–21]) suggest hadronic uncertainties to be less than 10%. For example, Ref. [21] quotes $a_{\eta' K} - a_{\psi K} = 0.01 \pm 0.01$ and $a_{\phi K} - a_{\psi K} = 0.02 \pm 0.01$. The measurements of the time dependent CP asymmetries in the η' and ϕ modes, yield $a_{\eta' K} = 0.61 \pm 0.07$ and $a_{\phi K} = 0.39 \pm 0.18$. The latter deviates from the SM prediction $a_{s\bar{s}s} = 0.78 \pm 0.04$ at the two sigma level.

It is rather curious that all the time dependent CP asymmetries in $b \to s\bar{s}s$ have been measured to be somewhat smaller than the $B \to J/\psi K_s$ asymmetry. If we naively compute the average of the CP asymmetries in all the $b \to s\bar{s}s$ modes, even though only three of the modes are very clean and others may have $O(10\%)$ uncertainties, one then finds $[a_{s\bar{s}s}]_{\rm average} = 0.52 \pm 0.05$ with a deviation of about 4σ from the SM prediction and about 3σ from the value directly measured by the ψK_s method.

For the sake of completion, we also note that just averaging over the three clean modes gives $a_{clean} = 0.57 \pm 0.06$. Since in so far as the SM is concerned, $\sin 2\beta$ may be measured either by these three clean penguin modes or by the $J/\psi K_s$ modes, the best "SM" direct measurement of $\sin 2\beta$ is given by the average over the $(J/\psi, \phi, \eta', K_s K_s) K_s$ modes: we thus find $\sin 2\beta = 0.66 \pm 0.02$ which is again about 2.5σ from the SM prediction of 0.78 ± 0.04.

CP asymmetries in $B \to K\pi$

The QCD–factorization predictions for the individual CP asymmetries in $B \to K\pi$ decays [30, 31] are extremely sensitive to non–factorizable (hence model dependent) effects and cannot be used to directly constrain the SM. Luckily it turns out that, in the calculation of the difference between the CP asymmetries in $B^+ \to K^+\pi^-$ and $B^- \to K^-\pi^0$, most model dependent uncertainties cancel and the QCD–factorization prediction is quite reliable. The magnitude

$\lvert V_{ub}/V_{cb}\rvert = 0.1036 \pm 0.0074$ [25]	$\varepsilon_K^{\rm exp} = (2.280 \pm 0.013)\ 10^{-3}$
$\Delta m_{B_s}^{\rm exp} = (17.77 \pm 0.10 \pm 0.07){\rm ps}^{-1}$ [26]	$a_{\psi K_s}^{\rm exp} = 0.675 \pm 0.026$
$\Delta m_{B_d}^{\rm exp} = (0.507 \pm 0.005){\rm ps}^{-1}$	$\hat{B}_K = 0.79 \pm 0.04 \pm 0.08$ [27, 28]
$\xi_s = 1.210^{+0.047}_{-0.035}$ [29]	

Table 1: Inputs that we use in the unitarity triangle fit.

of this cancelation is apparent in the comparison between the predictions for the individual asymmetries and for their difference. The results of Ref. [31] read:

$$A_{CP}(B^- \to K^-\pi^0) = \left(7.1^{+1.7+2.0+0.8+9.0}_{-1.8-2.0-0.6-9.7}\right)\% \quad (1)$$

$$A_{CP}(\bar{B}^0 \to K^-\pi^+) = \left(4.5^{+1.1+2.2+0.5+8.7}_{-1.1-2.5-0.6-9.5}\right)\% \ , \quad (2)$$

where the first error corresponds to uncertainties on the CKM parameters and the other three correspond to variation of various hadronic parameters; in particular, the fourth one corresponds to the unknown power corrections. The main point is that the uncertainties in the two asymmetries are highly correlated. This fact is reflected in the prediction for their difference; we find:

$$\Delta A_{CP} = A_{CP}(B^- \to K^-\pi^0) - A_{CP}(\bar{B}^0 \to K^-\pi^+) = (2.5 \pm 1.5)\% \ . \quad (3)$$

In evaluating the theory error for this case, we followed the analysis presented in Ref. [31] and even allowed for some extreme scenarios (labeled S1-S4 in Ref. [31]) in which several inputs are simultaneously pushed to the border of their allowed ranges. The comparison of the SM prediction in Eq. (3) to the experimental determination of the same quantity [14]

$$\Delta A_{CP}^{\rm exp} = (14.4 \pm 2.9)\% \ , \quad (4)$$

yields a 3.5σ effect.

Muon $g-2$

The muon anomalous magnetic moment has been thoughtfully investigated in the literature. The most up–to–date calculation of the SM prediction suffers from model dependent uncertainties in the calculation of the light–by–light hadronic contribution; nevertheless, all the estimates (see, for instance, Ref. [32] for a collection of results) point to a SM prediction that is lower than the experimental measurement by about three sigmas. The inconsistency between the extraction of the hadronic contribution to the vacuum polarization from τ and e^+e^- data is still an open question. We note, however, that the use of the former requires model dependent

assumptions on the size of isospin breaking effects; for this reason, most analyses prefer not to include τ decay data. The most recent theory estimate is [33]

$$a_\mu^{\rm SM} = 116591785(61) \times 10^{-11} \ , \tag{5}$$

while the present measurement is [34, 35]:

$$a_\mu^{\rm SM} = 116592080(63) \times 10^{-11} \ . \tag{6}$$

The discrepancy is at the 3σ level.

Forward–backward asymmetry in $Z \to b\bar{b}$

The LEP measurement of the forward–backward asymmetry in $Z \to b\bar{b}$ reads $A_{fb}^{0,b} = 0.0992 \pm 0.0016$. The discrepancy between this experimental result and the central value of the SM fit, $(A_{fb}^{0,b})_{SM} = 0.1038$ is at the 3 sigma level. Care has to be taken in interpreting this result because the indirect determination of $A_{fb}^{0,b}$ from the forward–backward Left–Right asymmetry (A_b) is compatible with the SM prediction at 1 sigma.

Overview: the pull table

Let us give a global view of the status of the Standard Model by collecting most measurements sensitive to the flavor sector and their deviation from the corresponding SM predictions*. Note that several of the entries indicate deviation from the SM in the 2.5 - 3.5 σ range.

Observable	Experiment	SM	Pull
$\mathcal{B}(B \to X_s\gamma) \times 10^4$	3.55 ± 0.26	2.98 ± 0.26	+1.6
$\mathcal{B}(B \to \tau\nu_\tau) \times 10^4$	1.31 ± 0.48	0.85 ± 0.13	+0.9
Δm_{B_s} (ps^{-1})	17.77 ± 0.12	18.6 ± 2.3	-0.4
$a_{\psi K}$	0.675 ± 0.026	0.78 ± 0.04	-2.0
$a_{\phi K}$	0.39 ± 0.18	0.80 ± 0.04	-2.2
$a_{\eta' K}$	0.61 ± 0.07	0.79 ± 0.04	-2.0
$a_{K_s K_s K_s}$	0.51 ± 0.21	0.80 ± 0.04	-1.3
$a_{(\phi K+\eta' K+KKK)}$	0.57 ± 0.06		-2.9
$a_{(\phi K+\eta' K+KKK+\psi K)}$	0.66 ± 0.02		-2.6

*See Sec. 5 for a detailed discussion of the various observables

$[a_{s\bar{s}s}]_{\text{naiveaverage}}$	0.52 ± 0.05		-3.7
$\Delta\Gamma_s/\Gamma_s$	0.27 ± 0.08	0.147 ± 0.060	+1.2
ΔA_{CP}	0.144 ± 0.029	0.025 ± 0.015	+3.6
$a_\mu \times 10^{11}$	1.16592080(63)	1.16591785(61)	+3.4
$A_{fb}^{0,b}$	0.0992 ± 0.0016	0.1038	-2.9
$\lvert V_{ub}\rvert \times 10^3$	4.31 ± 0.30	3.44 ± 0.16	+2.6

In the next section we will introduce a particular new physics model, the two Higgs doublet model for the top quark (T2HDM), and see how well it can accommodate the above mentioned deviations.

3 The two Higgs doublet model for the top quark

The T2HDM is a special case of type-III 2HDM. It was first proposed in Ref. [6] and subsequently analyzed in Refs. [7, 8, 36]. In this model, one of the Higgses has only interactions involving the right–hand top, while the other one couples to the remaining right–handed fermions (but not to the top). The main motivation for this model is to give the top quark a unique status, thus explaining in a natural way its large mass; hence large values of $\tan\beta_H$ (the ratio of the vev's of the two Higgs fields) are preferred. As we will see in the following, a consequence of the peculiar structure of the T2HDM is that the model contains two additional flavor changing complex couplings on top of the standard 2HDM parameters.

The Yukawa interactions of the quarks with the Higgs fields are:

$$\mathcal{L}_Y = -\bar{Q}_L H_1 Y_d d_R - \bar{Q}_L \tilde{H}_1 Y_u \mathbb{1}^{(12)} u_R - \bar{Q}_L \tilde{H}_2 Y_u \mathbb{1}^{(3)} u_R + \text{h.c.} \,, \tag{7}$$

where H_i are the two doublets, $\tilde{H}_i = i\sigma^2 H_i^*$, $Y_{u,d}$ are Yukawa matrices, $\mathbb{1}^{(12)} = \text{diag}(1,1,0)$, and $\mathbb{1}^{(3)} = \text{diag}(0,0,1)$. After the electroweak symmetry breaking, the neutral components of Higgs doublets receive two independent complex vev's, $v_1/\sqrt{2} = ve^{i\phi_1}\cos\beta_H/\sqrt{2}$ and $v_2/\sqrt{2} = ve^{i\phi_2}\sin\beta_H/\sqrt{2}$, whose ratio is $\tan\beta_H \equiv |v_2/v_1|$.

The quark mass matrices in the mass eigenstate basis are:

$$m_d = D_L^\dagger \left(\frac{v_1^*}{\sqrt{2}} Y_d\right) D_R \,, \tag{8}$$

$$m_u = U_L^\dagger \left(\frac{v_1^*}{\sqrt{2}} Y_u \mathbb{1}^{(12)} + \frac{v_2^*}{\sqrt{2}} Y_u \mathbb{1}^{(3)}\right) U_R \,, \tag{9}$$

where $m_{u,d}$ are diagonal, $U_{L,R}$ and $D_{L,R}$ are unitary matrices and $V = U_L^\dagger D_L$ is the CKM matrix. The charged and neutral Higgses interactions read:

$$\begin{aligned}
\mathcal{L}_Y^C &= -\bar{u}_L V m_d d_R \frac{H_1^+}{v_1^*/\sqrt{2}} - \bar{u}_R \left(m_u V \frac{H_1^+}{v_1^*/\sqrt{2}} + \Sigma^\dagger V \left[\frac{H_2^+}{v_2^*/\sqrt{2}} - \frac{H_1^+}{v_1^*/\sqrt{2}} \right] \right) d_L + \text{h.c.} \\
&= \frac{g_2}{\sqrt{2} m_W} \bar{u} \Big[\left(-V m_d P_R + m_u V P_L \right) \left(G^+ - \tan\beta_H H^+ \right) + \Sigma^\dagger V P_L (\tan\beta_H + \cot\beta_H) H^+ \Big] d + \text{h.c.} \\
&\equiv \bar{u}_L (P_{LR}^H H^+ + P_{LR}^G G^+) d_R + \bar{u}_R (P_{RL}^H H^+ + P_{RL}^G G^+) d_L + \text{h.c.} \qquad (10)
\end{aligned}$$

$$\begin{aligned}
\mathcal{L}_Y^N &= -\bar{d}_L m_d d_R \frac{H_1^{0*}}{v_1^*/\sqrt{2}} - \bar{u}_L \left(m_u \frac{H_1^{0*}}{v_1^*/\sqrt{2}} + \Sigma \left[\frac{H_2^{0*}}{v_2^*/\sqrt{2}} - \frac{H_1^{0*}}{v_1^*/\sqrt{2}} \right] \right) u_R + \text{h.c.} \\
&= \frac{g_2 \tan\beta_H}{2 m_W} \Bigg[\left(\bar{d}_L m_d d_R + \bar{u}_L m_u u_R \right) \frac{h^0 \sin\alpha_H - H^0 \cos\alpha_H}{\sin\beta_H} + i \left(\bar{d}_L m_d \gamma_5 d_R + \bar{u}_L m_u \gamma_5 u_R \right) A^0 \\
&\quad - \bar{u}_L \Sigma^\dagger u_R \frac{H^0 \sin(\alpha_H - \beta_H) + h^0 \cos(\alpha_H - \beta_H)}{\sin^2\beta_H} - i(1 + \cot^2\beta_H) \bar{u}_L \Sigma^\dagger \gamma_5 u_R A^0 \Bigg] + \text{h.c.} \\
&\equiv \bar{d}_L (P_d^{h^0} h^0 + P_d^{H^0} H^0 + i\gamma_5 P_d^{A^0} A^0) d_R + \bar{u}_L (P_u^{h^0} h^0 + P_u^{H^0} H^0 + i\gamma_5 P_u^{A^0} A^0) u_R + \text{h.c.}\ , \qquad (11)
\end{aligned}$$

where $\Sigma \equiv m_u U_R^\dagger \mathbb{1}^{(3)} U_R$. The would be Goldstone boson $G^\pm$, the charged Higgs $H^\pm$, the heavy and light scalars H^0 and h^0, and the pseudoscalar A^0 are given by:

$$\begin{aligned}
\begin{pmatrix} H_1^0 e^{-i\phi_1} \\ H_2^0 e^{-i\phi_2} \end{pmatrix} &= \frac{1}{\sqrt{2}} \left[R_{\alpha_H} \begin{pmatrix} H^0 \\ h^0 \end{pmatrix} + i R_{\beta_H} \begin{pmatrix} G^0 \\ A^0 \end{pmatrix} + \begin{pmatrix} |v_1| \\ |v_2| \end{pmatrix} \right] , \qquad (12) \\
\begin{pmatrix} H_1^\pm \\ H_2^\pm \end{pmatrix} &= R_{\beta_H} \begin{pmatrix} G^\pm \\ H^\pm \end{pmatrix} , \qquad (13)
\end{aligned}$$

with

$$R_\omega = \begin{pmatrix} \cos\omega & -\sin\omega \\ \sin\omega & \cos\omega \end{pmatrix} \qquad (14)$$

The explicit expressions for the charged Higgs couplings are:

$$\begin{aligned}
P_{LR}^H &= \frac{g_2}{\sqrt{2} m_W} \tan\beta_H\ V\ m_d\ , \qquad (15) \\
P_{RL}^H &= \frac{g_2}{\sqrt{2} m_W} \tan\beta_H \left[(1 + \tan^{-2}\beta_H) \Sigma^\dagger - m_u \right] V\ , \qquad (16) \\
P_{LR}^G &= -\frac{g_2}{\sqrt{2} m_W} V\ m_d\ , \qquad (17) \\
P_{RL}^G &= \frac{g_2}{\sqrt{2} m_W} m_u\ V\ . \qquad (18)
\end{aligned}$$

The explicit expressions for the neutral Higgs couplings are:

$$P_u^{h^0} = \frac{g_2 \tan\beta_H}{2m_W}\left(m_u \frac{\sin\alpha_H}{\sin\beta_H} - \Sigma^\dagger \frac{\cos(\alpha_H-\beta_H)}{\sin^2\beta_H}\right) \tag{19}$$

$$P_u^{H^0} = -\frac{g_2 \tan\beta_H}{2m_W}\left(m_u \frac{\cos\alpha_H}{\sin\beta_H} + \Sigma^\dagger \frac{\sin(\alpha_H-\beta_H)}{\sin^2\beta_H}\right) \tag{20}$$

$$P_u^{A^0} = \frac{g_2 \tan\beta_H}{2m_W}\left(m_u - \frac{1+\tan^2\beta_H}{\tan^2\beta_H}\Sigma^\dagger\right) \tag{21}$$

$$P_d^{h^0} = \frac{g_2 \tan\beta_H}{2m_W} m_d \frac{\sin\alpha_H}{\sin\beta_H} \tag{22}$$

$$P_d^{H^0} = -\frac{g_2 \tan\beta_H}{2m_W} m_d \frac{\cos\alpha_H}{\sin\beta_H} \tag{23}$$

$$P_d^{A^0} = \frac{g_2 \tan\beta_H}{2m_W} m_d \ . \tag{24}$$

From the definition of Σ it is clear that only the third row of the matrix U_R is relevant up to an overall phase (i.e. we can take $(U_R)_{33}$ real). Taking into account the unitarity constraint, it follows that Σ depends on only 4 real parameters. This statement can be explicitly verified by employing the most general parametrization of a unitary matrix: $U = P_1 V P_2$, where P_i are diagonal phase matrices and V is a unitary matrix that depends on three angles and a single phase (e.g. it is CKM-like). The third row of this matrix can always be written as:

$$U_R = \begin{pmatrix} * & * & * \\ * & * & * \\ \hat{\xi}'\sqrt{1-|\hat{\xi}|^2} & \hat{\xi} & \sqrt{1-|\hat{\xi}|^2}\sqrt{1-|\hat{\xi}'|^2} \end{pmatrix} \tag{25}$$

where $\hat{\xi}$ and $\hat{\xi}'$ are complex parameters with $|\hat{\xi}^{(\prime)}| \leq 1$. In models based on dynamical top-condensation [37,38] and top-color [39,40] the parameters $\hat{\xi}^{(\prime)}$ are naturally of order $\epsilon_{ct} = m_c/m_t$ (see also Ref. [41]); for this reason we introduce new parameters $\xi^{(\prime)} = \epsilon_{ct}\hat{\xi}^{(\prime)}$ with $\xi^{(\prime)} = O(1)$. Neglecting terms proportional to the u-quark mass, the matrix Σ reads:

$$\begin{aligned} \frac{\Sigma}{m_t} &= \begin{pmatrix} 0 & 0 & 0 \\ \epsilon_{ct}^3 \xi^* \xi' \sqrt{1-|\hat{\xi}|^2} & \epsilon_{ct}^3 |\xi|^2 & \epsilon_{ct}^2 \xi^* \sqrt{1-|\hat{\xi}|^2}\sqrt{1-|\hat{\xi}'|^2} \\ \epsilon_{ct}\xi'\sqrt{1-|\hat{\xi}'|^2}(1-|\hat{\xi}|^2) & \epsilon_{ct}\xi\sqrt{1-|\hat{\xi}'|^2}\sqrt{1-|\hat{\xi}'|^2} & (1-|\hat{\xi}|^2)(1-|\hat{\xi}'|^2) \end{pmatrix} \\ &= \begin{pmatrix} 0 & 0 & 0 \\ 0 & 0 & \epsilon_{ct}^2 \xi^* \\ \epsilon_{ct}\xi' & \epsilon_{ct}\xi & 1 \end{pmatrix} \times + O\left(\epsilon_{ct}^3, \frac{m_u}{m_t}\right) \ . \end{aligned} \tag{26}$$

From Eq. (10) we find the following charged Higgs interactions between right-handed up quarks and left-handed down quarks:

$$\frac{g_2 m_c \tan\beta_H}{\sqrt{2} m_W} \begin{pmatrix} \xi'^* V_{td} & \xi'^* V_{ts} & \xi'^* V_{tb} \\ \xi^* V_{td} - V_{cd} & \xi^* V_{ts} - V_{cs} & \xi^* V_{tb} - V_{cb} \\ V_{td}\cot^2\beta_H/\epsilon_{ct} + \epsilon_{ct}\xi V_{cd} & V_{ts}\cot^2\beta_H/\epsilon_{ct} + \epsilon_{ct}\xi V_{cs} & V_{tb}\cot^2\beta_H/\epsilon_{ct} \end{pmatrix} \ . \tag{27}$$

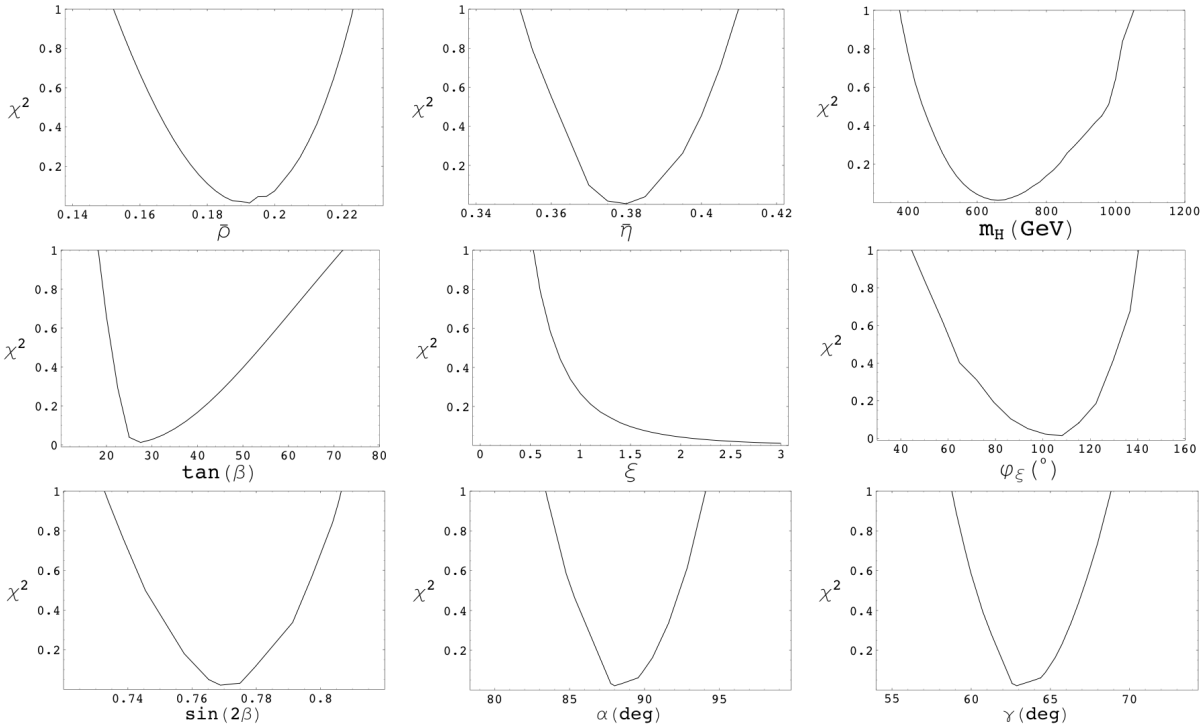

Figure 2: Dependence of χ^2_{min} on $\bar{\rho}$, $\bar{\eta}$, $m_{H^\pm}$, $\tan\beta_H$, $|\xi|$, φ_ξ, $\sin 2\beta$, α and γ. For each value of the parameter on the x-axis, we minimize the chi-square with respect to all the others (including $\bar{\rho}$ and $\bar{\eta}$.

In particular $\bar{t}_R q_L$ (q=d,s) interactions are dominated by the ξ term for $\tan\beta_H > 10$. In conclusion, the parameters of the models are: $\tan\beta_H$, α_H, $m_{H^\pm}$, m_{H^0}, m_{h^0}, m_A^0, ξ and ξ'.

Finally let us comment on the renormalization scheme of the quark masses that appear in Eqs. (10) and (11). In the calculation of the additional matching conditions to various operators we integrate out the charged and neutral higgses at some high scale $\mu_0 \sim O(m_W, m_t)$; therefore, it is most natural to evaluate all the relevant couplings in the $\overline{MS}$ scheme at the high scale. This observation has a very strong impact on the phenomenology of the T2HDM because of the strong renormalization scale dependence of the charm quark: $m_c^{\overline{MS}}(\mu_0)/m_c^{\rm pole} \simeq 0.45$.

4 Global analysis

In this section we present the results of global χ^2 fit of the T2HDM parameter space. Here we just focus on the outcome of the fit and investigate how well the T2HDM can answer to the problems we collected in Sec. 2. A detailed discussion of the various observables that we consider is given in Secs. 5 and 6), in which we collect the experimental data and the analytic formulae required to calculate T2HDM effects. In those sections we also show the separate impact of each observable on the T2HDM parameter space.

We classify the various observables we consider according to whether neutral Higgs exchange

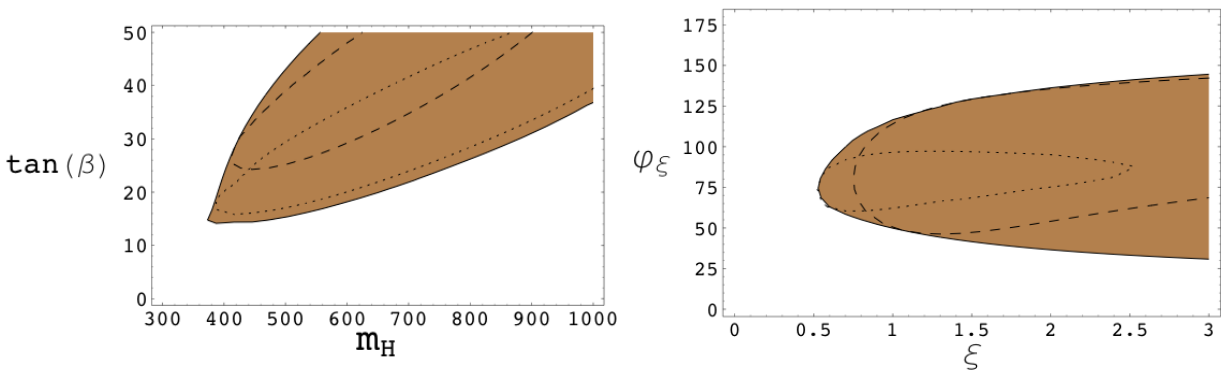

Figure 3: Contour plots corresponding to $\chi^2_{min} \leq 1$ in the $(m_{H^\pm}, \tan\beta_H)$ and (ξ, φ_ξ) planes. For each point on the contour, we minimize with respect to all other variables. The dashed and dotted contours correspond to $\xi = (1, 2)$ and $\tan\beta_H = (30, 50)$ for the left and right plot, respectively.

contributions are relevant or not. In the latter case, the parameter count of the model is reduced to the sole $\tan\beta_H$, $m_{H^\pm}$, ξ and ξ'. Observables insensitive to the neutral Higgs sector of the T2HDM include: rare B decays ($b \to s\gamma$, $b \to s\ell^+\ell^-$, $B \to \tau\nu$), neutral meson mixing (K, B_d, B_s, D), various CP asymmetries (time–dependent asymmetries in $b \to c\bar{c}s$ and $b \to s\bar{s}s$ decays, asymmetries in flavor specific B decays, direct asymmetries in the $B \to K\pi$ system) and the neutron electric dipole moment (EDM). Among those observables that display some sensitivity to the neutral Higgs sector we consider the muon anomalous magnetic moment, $\Delta\rho$ and the $Z \to b\bar{b}$ vertex (R_b and the forward–backward asymmetry A_b).

In the χ^2 analysis we focus on the first set of observables and treat separately the $\xi' = 0$ and $\xi' \neq 0$ cases. In fact, the parameter ξ' is related exclusively to transitions between the first and third generations and impacts only $B \to \tau\nu$, $D\bar{D}$ mixing and the neutron EDM, while being completely negligible in all other observables. The T2HDM phenomenology of observables dominated by neutral Higgs exchanges is very similar to the one of a regular Two Higgs Doublet Model and we will briefly summarize it in Sec. 6.

Our general strategy is to include directly into the fit only processes for which the theory error is reasonably under control; once a region of the T2HDM parameter space has been singled out, we look at the other observables.

$\xi' = 0$

As a first step we set $\xi' = 0$. The χ^2 that we consider includes the following quantities: $|V_{ub}/V_{cb}|$, $\Delta M_{B_s}/\Delta M_{B_d}$, $a_{\psi K}$, ε_K, $B \to X_s\gamma$, $B \to \tau\nu$. The resulting function depends on the CKM parameters $\bar{\rho}$ and $\bar{\eta}$, and on the T2HDM parameters $m_{H^\pm}$, $\tan\beta_H$, $\xi = |\xi|e^{i\varphi_\xi}$.

Note that, without the inclusion of T2HDM contributions, the overall χ^2–fit in the SM is relatively poor ($\chi^2_{min} \sim 6$). Once T2HDM effects are included, the fit improves drastically and we find $\chi^2_{min} \sim 0$. This implies that this set of measurements singles out a clear sector of the parameter space not compatible with the T2HDM decoupling limit. In Fig. 1 we show the

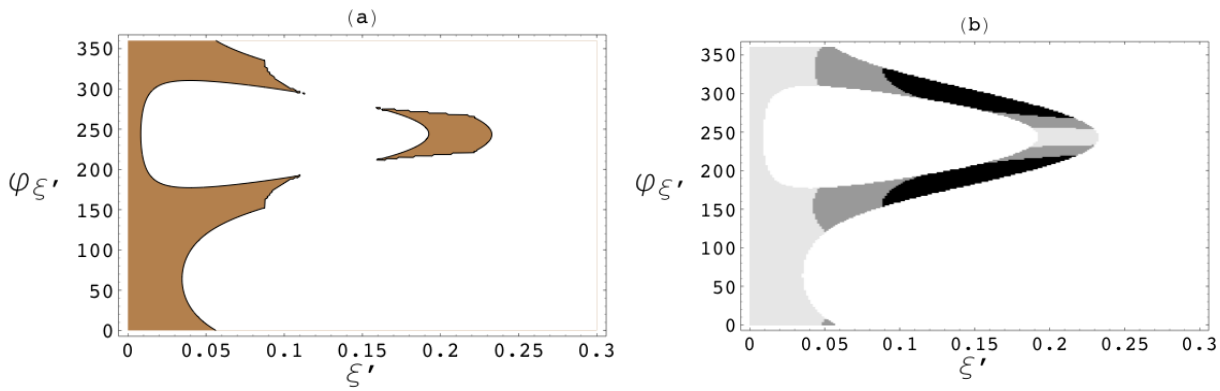

Figure 4: Contour plot corresponding to $\chi^2_{min} \leq 1$ in the $(\xi', \varphi_{\xi'})$ plane. The rest of the parameters are chosen so to minimize the χ^2 for $\xi' = 0$. In the plot on the right the light gray, dark gray and black regions correspond to a neutron–EDM (given in units of 10^{-26} e cm) smaller than 3, between 3 and 6.3, and bigger than 6.3, respectively.

unitarity triangle fit in the Standard Model; note, in particular, the tension between the black contour and the constraint from $a_{\psi K}$ (not included in the fit). In Fig. 2, we show the actual dependence of the full χ^2 on the CKM angles and the four T2HDM parameters. The 68% C.L. intervals that we find are:

$$m_{H^\pm} = \left(660^{+390}_{-280}\right) \text{ GeV} , \tag{28}$$

$$\tan\beta = 28^{+44}_{-8} , \tag{29}$$

$$\xi > 0.5 , \tag{30}$$

$$\varphi_\xi = \left(110^{+30}_{-65}\right)^o , \tag{31}$$

$$\bar{\rho} = 0.19 \pm 0.035 , \tag{32}$$

$$\bar{\eta} = 0.38 \pm 0.03 . \tag{33}$$

The corresponding ranges for the three UT angles are:

$$\sin(2\beta) = 0.77 \pm 0.04 , \tag{34}$$

$$\alpha = (89 \pm 6)^o , \tag{35}$$

$$\gamma = (64 \pm 5)^o . \tag{36}$$

In Fig. 3 we show the correlation between these parameters; the shaded areas correspond to $\chi^2_{min} \leq 1$ and their projections on the axes yield the corresponding 1σ regions.

We are now in the position of evaluating how well the T2HDM does with respect to the pull table we introduced in Sec. 2. From the outcome of the fit it is clear that the T2HDM can easily accommodate the deviations in $B \to X_s\gamma$, $B \to \tau\nu$, $a_{\psi K}$ and $|V_{ub}|$. Unfortunately, for $m_{H^\pm} > 400$ GeV, it seems quite difficult to accommodate the effect required to reconcile the CP asymmetries in $B \to (\eta', \phi)K_S$ with experimental data (see Fig. 13 in Sec. 5.4). The impact

of the T2HDM on ΔM_{B_s} is not very large and is perfectly compatible with the present experimental determination. Finally we do not find any large contribution to the CP asymmetries in $B \to K\pi$, hence within the T2HDM the 3.6σ observed deviation remains unexplained.

Let us note that the solution of the $|V_{ub}|$ vs $a_{\psi K}$ puzzle is achieved via sizable and highly correlated contributions to both $a_{\psi K}$ and ε_K: after the inclusion of the constraints from $B \to X_s\gamma$ and $B \to \tau\nu$, the solution of this puzzle was a crucial bonus that we could not enforce (due to the extremely reduced number of parameters that we are considering).

Finally we point out that T2HDM effects on $a_{\psi K}$ are caused by large complex contributions to the amplitude $\mathcal{A}(B \to J/\psi K_s)$ and not to the $B - \bar{B}$ mixing matrix element (i.e. M_{12}^d). Since the former is dominated by the tree–level transition $b \to c\bar{c}s$, any other process controlled by this quark–level decay will display similar large effects. This is particularly true for time dependent CP asymmetries in B_s decays. The $B_s \to J/\psi\ \eta'$ mode, for instance, is based on the $b \to c\bar{c}s$ amplitude, hence, in the naive factorization limit, the T2HDM contributions to its time dependent CP asymmetry must be identical to the corresponding ones in $B \to J/\psi K_s$. Therefore, the above χ^2 analysis predicts the T2HDM contribution to this asymmetry to be in the +10% range. Given that the SM expectation for this quantity is extremely small (the phase of the SM $B_s - \bar{B}_s$ amplitude is about one degree), the measurement of a large enhancement in the $B \to J/\psi K$ asymmetry is a clear indication for a resolution of the a_{psiK} puzzle via new physics in the amplitudes (as it is the case in the T2HDM).

$\xi' \neq 0$

In order to study the effects of non vanishing ξ', we fix the other parameters to the values that minimize the χ^2 we just studied; then we include contributions from $B \to \tau\nu$, $D\bar{D}$ mixing and the neutron EDM (for the latter two, we impose upper limits – see Secs. 5.3 and 5.7 for details). Note that without the inclusion of $B \to \tau\nu$, the fit for $\xi' = 0$ favors values of ξ smaller than 1 (the actual value that we use in the $\xi' \neq 0$ fit is $\xi \simeq 0.8$).

In Fig. 4, we plot the region of $(\xi', \varphi_{\xi'})$ plane for which this new χ^2 is smaller than 1. The main constraint comes from $B \to \tau\nu$, whose branching ratio is proportional to ξ'^2. It is interesting to dissect contributions to the neutron EDM: in the right plot in Fig. 4 the regions with increasing darkness correspond to a neutron-EDM (in units of 10^{-26} e cm) smaller than 3, between 3 and 6.3, and bigger than 6.3, respectively.

5 Observables: the charged Higgs sector

5.1 $B \to X_s\gamma$ and $B \to X_s\ell^+\ell^-$

The experimental world average from the CLEO [42], Belle [43, 44] and BaBar [45, 46] collaborations is given by [47]:

$$\mathrm{BR}(B \to X_s\gamma)_{E_\gamma > 1.6\mathrm{GeV}} = (3.55 \pm 0.24^{+0.09}_{-0.10} \pm 0.03) \times 10^{-4}\ . \tag{37}$$

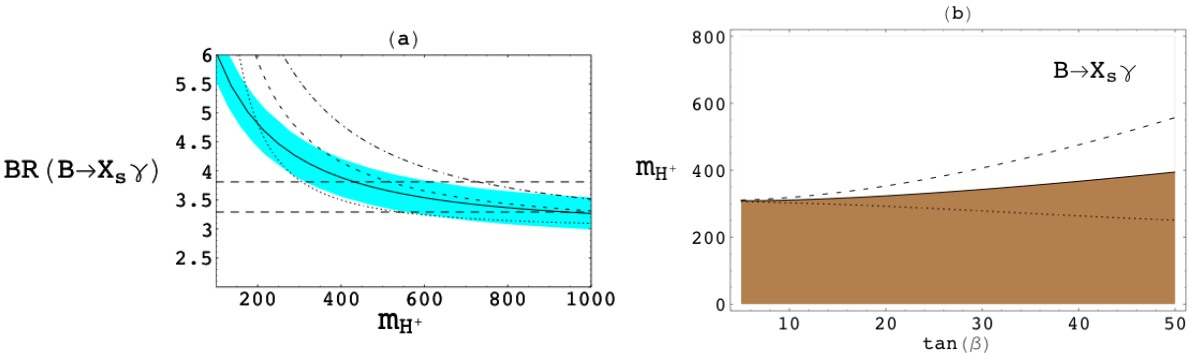

Figure 5: **Plot a**. $m_{H^\pm}$ dependence of the branching ratio $B \to X_s\gamma$ in units of 10^{-4}. Solid, dashed, dotted and dotted-dashed lines correspond to $(\tan\beta_H, \xi) = (10, 0)$, $(50, 0)$, $(50, 1)$ and $(50, -1)$, respectively. There is no appreciable dependence on ξ'. The two horizontal dashed lines are the experimental 68%C.L. allowed region. The blue region represents the theory uncertainty associated to the solid line (similar bands can be drown for the other cases). **Plot b**. Portion of the $(\tan\beta_H, m_{H^\pm})$ plane excluded at 68%C.L. by the $B \to X_s\gamma$ measurement. The shaded area corresponds to $\xi = 0$. The dotted and dashed lines show how this region changes for $\xi = 1$ and -1, respectively.

The $B \to X_s\ell^+\ell^-$ branching ratio has been recently measured by both Belle [48] and BaBar [49]; in the low dilepton invariant mass region, 1 GeV$^2 < m^2_{\ell\ell} <$ 6 GeV^2, the experimental results read

$$\mathcal{B}(B \to X_s\ell^+\ell^-) = (1.493 \pm 0.504^{+0.411}_{-0.321}) \times 10^{-6} \quad \text{(Belle)} , \tag{38}$$

$$\mathcal{B}(B \to X_s\ell^+\ell^-) = (1.8 \pm 0.7 \pm 0.5) \times 10^{-6} \quad \text{(BaBar)} . \tag{39}$$

This leads to a world average

$$\mathcal{B}(B \to X_s\ell^+\ell^-) = (1.60 \pm 0.51) \times 10^{-6} . \tag{40}$$

The effective Hamiltonian responsible for the transitions $b \to s\gamma$ and $b \to s\ell^+\ell^-$ is [50]

$$\mathcal{H}_{\text{eff}} = -4\frac{G_F}{\sqrt{2}} V_{tb}V^*_{ts}\left[\sum_{i=1}^{10} C_i(\mu)P_i(\mu) + \sum_{i=3}^{6} C_{iQ}(\mu)P_{iQ} + C_b(\mu)P_b\right] \tag{41}$$

where the most relevant operators are

$$P_7 = \frac{e}{16\pi^2} m_b(\bar{s}_L\sigma^{\mu\nu}b_R)F_{\mu\nu} , \tag{42}$$

$$P_8 = \frac{g}{16\pi^2} m_b(\bar{s}_L\sigma^{\mu\nu}T^a b_R)G^a_{\mu\nu} , \tag{43}$$

$$P_9 = (\bar{s}_L\gamma_\mu b_L)\sum_\ell(\bar{\ell}\gamma^\mu\ell) , \tag{44}$$

$$P_{10} = (\bar{s}_L\gamma_\mu b_L)\sum_\ell(\bar{\ell}\gamma^\mu\gamma_5\ell) . \tag{45}$$

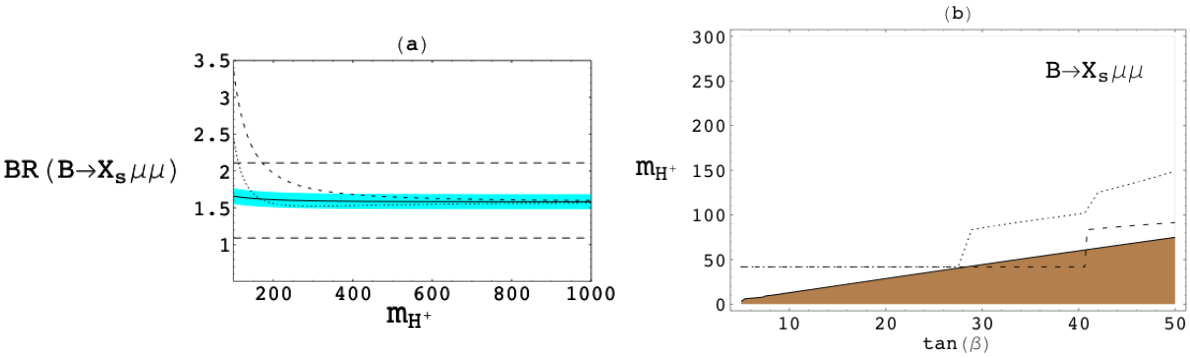

Figure 6: **Plot a**. $m_{H^\pm}$ dependence of the branching ratio $B \to X_s\mu\mu$ in units of 10^{-6}. Solid, dashed and dotted lines correspond to $(\tan\beta_H, \xi) = (10, 0)$, $(50, 1)$ and $(50, -1)$, respectively. There is no appreciable dependence on ξ'. The two horizontal dashed lines are the experimental 68%C.L. allowed region. The blue region represents the theory uncertainty associated to the solid line (similar bands can be drown for the other cases). **Plot b**. Portion of the $(\tan\beta_H, m_{H^\pm})$ plane excluded at 68%C.L. by the $B \to X_s\mu\mu$ measurement. The shaded area corresponds to $\xi = 0$. The dotted and dashed lines show how this region changes for $\xi = 1$ and -1, respectively.

The leading order charged Higgs contributions in the T2HDM to the Wilson coefficients $C_{7,8,9,10}$ have been in explicitly calculated in Refs. [7,8,36,51] (see Eqs. (7-15) of Ref. [36]). The formula for the new physics contribution to C_7 is:

$$\begin{aligned} C_7^{\rm NP}(m_W) &= \left(-V_{tb}V_{ts}^*\frac{4G_F}{\sqrt{2}}\right)^{-1}\sum_{i=u,c,t}\left\{\frac{(P^H_{LR})_{i3}(P^H_{RL})^*_{i2}}{m_b\, m_{u_i}}B(y_i) + \frac{(P^H_{RL})_{i3}(P^H_{RL})^*_{i2}}{m^2_{u_i}}\frac{A(y_i)}{6}\right\} \\ &\simeq -\Big[B(y_t) + \tan^2\beta_H\; B(y_c)\Big] + \xi^*\tan^2\beta_H\left[-\frac{1}{6}\frac{V_{tb}}{V_{cb}}A(y_c) - \epsilon^2_{ct}\frac{V_{cs}}{V_{ts}}B(y_t)\right]\,, \quad (46) \end{aligned}$$

where both quantities in square brackets are positive for any choice of $\tan\beta_H$ and $m_{H^\pm}$, $y_a = m_a^2/m^2_{H^\pm}$ and the loop-functions A and B are given in Ref. [36].

A numerical formula for the calculation of the $B \to X_s\gamma$ branching ratio is given in Ref. [52, 53]:

$$\begin{aligned} \mathcal{B}(\bar{B} \to X_s\gamma)^{\rm th}_{E_\gamma > 1.6\ {\rm GeV}} &= 10^{-4}\Big[2.98 + 4.743\,|\delta C_7|^2 + 0.789\,|\delta C_8|^2 + {\rm Re}\Big(\\ &(-7.184 + 0.612\,i)\,\delta C_7 + (-2.225 - 0.557\,i)\,\delta C_8 + (2.454 - 0.884\,i)\,\delta C_8\,\delta C_7^*\Big)\Big]\,, \quad (47) \end{aligned}$$

where the leading Wilson coefficients at the high scale are given by $C_i^{(0)}(\mu_0) = C^{(0)}_{i,SM}(\mu_0) + \delta C_i$ and the next-to-leading matching conditions are assumed not to receive any new physics contribution, $C_i^{(1)}(\mu_0) = C^{(1)}_{i,SM}(\mu_0)$. The formula above has been obtain by observing that using the same numerical inputs of Ref. [54, 55] and taking $(\mu_c, \mu_b,\, mu_0) = (1.5, 2.5, 120)$ GeV, the NLO central value of the branching ratio coincides with the NNLO one. Eq. (47) also

include an estimate of the new class of power corrections identified in Ref. [56] and of the analysis of the photon energy spectrum presented in Ref. [57]. The analyses in Refs. [54, 57] yield $\mathcal{B}(B \to X_s\gamma) = (2.98 \pm 0.26) \times 10^{-4}$; we will therefore assign a theoretical error of 8.7% to the central values calculated in Eq. (47).

The Standard Model matching conditions and numerical formulae for the calculation of the integrated $B \to X_s\ell^+\ell^-$ branching ratios is given in Ref. [50]:

$$\begin{aligned}
\mathcal{B}_{\ell\ell} \;=\; & \Big[\, 2.1913 - 0.001655\, \mathcal{I}(R_{10}) + 0.0005\, \mathcal{I}(R_{10}R_8^*) + 0.0535\, \mathcal{I}(R_7) + 0.02266\, \mathcal{I}(R_7R_8^*) \\
& +0.00496\, \mathcal{I}(R_7R_9^*) + 0.00513\, \mathcal{I}(R_8) + 0.0261\, \mathcal{I}(R_8R_9^*) - 0.0118\, \mathcal{I}(R_9) \\
& -0.5426\, \mathcal{R}(R_{10}) + 0.0281\, \mathcal{R}(R_7) + 0.0153\, \mathcal{R}(R_7R_{10}^*) + 0.06859\, \mathcal{R}(R_7R_8^*) \\
& -0.8554\, \mathcal{R}(R_7R_9^*) - 0.00866\, \mathcal{R}(R_8) + 0.00185\, \mathcal{R}(R_8R_{10}^*) - 0.0981\, \mathcal{R}(R_8R_9^*) \\
& +2.7008\, \mathcal{R}(R_9) - 0.10705\, \mathcal{R}(R_9R_{10}^*) + 10.7687\, |R_{10}|^2 + 0.2889\, |R_7|^2 \\
& +0.00381\, |R_8|^2 + 1.4892\, |R_9|^2 \,\Big] \times 10^{-7}\ . \qquad (48)
\end{aligned}$$

where $R_i \equiv C_i(\mu_0)/C_i^{\rm SM}(\mu_0)$. The SM prediction is $BR(B \to X_s\ell^+\ell^-) = (1.59 \pm 0.11)10^{-6}$ and we will assign a theoretical error of 6.9% to the central values calculated in Eq. (48).

The impact that the $B \to X_s\gamma$ and $B \to X_s\ell\ell$ measurements have on the T2HDM parameter space is shown in Figs. 5 and 6. In Fig. 5a we plot the $B \to X_s\gamma$ branching ratio as a function of the charged Higgs mass for various choices of $\tan\beta_H$ and ξ. The $\tan\beta_H$ dependence of the charged Higgs contributions to C_7 is not very strong as it follows from the proximity of the solid and dashed curves. The ξ dependence is, on the other hand, much stronger; here we plot results for $\xi = (1, -1)$ (other choices of the phase yield in between curves). This can be seen explicitly in Fig. 5b, where we plot the allowed region at 68% C.L. in the $(\tan\beta_H, m_{H^\pm})$ plane for various choices of ξ. Comparison of the plots in Figs. 5 and 6 shows that $B \to X_s\ell\ell$ does not provide additional constraints on the parameter space.

5.2 Neutral mesons mixing

The off-diagonal element of the neutral K-mesons mass matrix is $M_{12}^* = \langle \overline{K}^0 \,|\mathcal{H}_{\rm eff}|\, K^0\rangle/(2m_K)$, where the effective Hamiltonian is

$$\mathcal{H}_{\rm eff} \;=\; \frac{G_F^2 m_W^2}{16\pi^2}\,(V_{ts}^*V_{td})^2 \sum_a C_a(\mu) Q_a\ , \qquad (49)$$

with

$$\begin{aligned}
Q^{\rm VLL} &= (\overline{s}_L\gamma_\mu d_L)\,(\overline{s}_L\gamma^\mu d_L) \\
Q_1^{\rm LR} &= (\overline{s}_L\gamma_\mu d_L)\,(\overline{s}_R\gamma_\mu d_R) \\
Q_2^{\rm LR} &= (\overline{s}_R d_L)\,(\overline{s}_L d_R) \qquad (50) \\
Q_1^{\rm SLL} &= (\overline{s}_R d_L)\,(\overline{s}_R d_L) \\
Q_2^{\rm SLL} &= (\overline{s}_R\sigma_{\mu\nu} d_L)\,(\overline{s}_R\sigma^{\mu\nu} d_L)\ .
\end{aligned}$$

$G_F = 1.1663910^{-5}$ GeV^{-2}	$\lambda = 0.2258 \pm 0.0014$ [27]
$m_W = 80.426$ GeV	$A = 0.818 \pm 0.012$ [27]
$m_K = 0.497648$ GeV	$\bar{\rho} = 0.197 \pm 0.031$ [27]
$m_c(m_c) = (1.224 \pm 0.017 \pm 0.054)$ GeV [58]	$\bar{\eta} = 0.351 \pm 0.020$ [27]
$m_{t,\text{pole}} = (171.4 \pm 2.1)$ GeV [59]	$\alpha_s^{\overline{MS}}(m_Z) = 0.1182 \pm 0.0027$ [60]
$\sin^2\theta_W = 0.2312$	$m_Z = 91.1876$ GeV
$m_b^{1S} = (4.68 \pm 0.03)$ GeV [61]	

Table 2: Numerical inputs that we use in the phenomenological analysis. Unless explicitly specified, they are taken from the PDG [25].

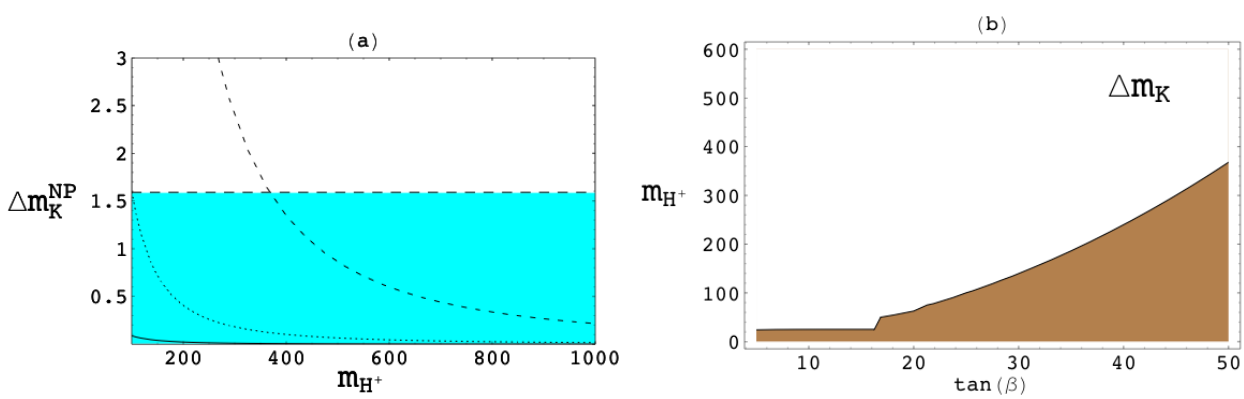

Figure 7: **Plot a**. $m_{H^\pm}$ dependence of the T2HDM contributions to Δm_K in units of 10^{-3} ps^{-1}. Solid, dotted and dashed lines correspond to $\tan\beta_H = 10$, 25 and 50, respectively. There is no appreciable dependence on ξ and ξ'. The horizontal dashed line corresponds to $\Delta m_K^{\rm NP} < 0.3\ \Delta m_K^{\rm exp}$. **Plot b**. Portion of the $(\tan\beta_H, m_{H^\pm})$ plane excluded by the $\Delta m_K^{\rm NP} < 0.3\ \Delta m_K^{\rm exp}$ constraint.

$r = 0.985$ [62]	$\eta_1 = 1.32 \left(\frac{1.3}{m_c(m_c)}\right)^{1.1} \pm 0.32$ [63]	$\hat{B}_K = 0.79 \pm 0.04 \pm 0.08$ [27]
$f_K = 0.159$ GeV [27]	$\eta_2 = 0.57 \pm 0.01$ [64]	$\eta_3 = 0.47 \pm 0.05$ [64]
$P_{1,K}^{LR} = -36.1$ [65]	$P_{2,K}^{LR} = 59.3$ [65]	$P_{1,K}^{SLL} = -18.1$ [65]
$P_{2,K}^{SLL} = -32.2$ [65]	$\Delta m_K^{\rm exp} = (5.301\ 10^{-3})$ ps^{-1}	$\varepsilon_K^{\rm exp} = (2.280 \pm 0.013)\ 10^{-3}$

Table 3: Inputs that we use in the phenomenological analysis of $K - \bar{K}$ mixing.

$f_{B_s}\sqrt{\hat{B}_s} = (0.281 \pm 0.021)$ GeV [66]	$m_{B_s} = 5.36675$ GeV	$m_{B_d} = 5.2794$ GeV
$f_{B_s}/f_{B_d} = 1.20 \pm 0.03$ [29]	$P_{1,B_d}^{LR} = -0.89$	$P_{1,B_s}^{LR} = -0.98$
$m_s^{\overline{MS}}(2\text{ GeV}) = (0.076 \pm 0.08)$ GeV [67]	$P_{2,B_d}^{LR} = 1.13$	$P_{2,B_s}^{LR} = 1.24$
$f_{B_d} = (0.216 \pm 0.022)$ GeV [29]	$P_{1,B_d}^{SLL} = -0.46$	$P_{1,B_s}^{SLL} = -0.51$
$\xi_s = f_{B_s}/f_{B_d}\sqrt{\hat{B}_s/\hat{B}_d} = 1.210^{+0.047}_{-0.035}$ [29]	$P_{2,B_d}^{SLL} = -0.90$	$P_{2,B_s}^{SLL} = -0.98$
$\Delta m_{B_d}^{\rm exp} = (0.507 \pm 0.005)$ps^{-1}	$\eta_B = 0.55$ [62]	$a_{\psi K_s}^{\rm exp} = 0.675 \pm 0.026$
$\Delta m_{B_s}^{\rm exp} = (17.77 \pm 0.10 \pm 0.07)$ps^{-1}		
$f_D = 0.165$ GeV [68]	$m_D = 1.8645$ GeV	$B_D = 0.78 \pm 0.01$ [69, 70]

Table 4: Inputs that we use in the phenomenological analysis of $B_q - \bar{B}_q$ and $D - \bar{D}$ mixing.

The additional operators $Q^{\rm VRR}$, $Q_1^{\rm SRR}$ and $Q_2^{\rm SRR}$ are obtained from $Q^{\rm VLL}$, $Q_1^{\rm SLL}$ and $Q_2^{\rm SLL}$ by replacing L with R. The effective Hamiltonians that describe B and B_s mixing are obtained via the replacements $(s,d) \to (b,d)$ and $(s,d) \to (b,s)$, respectively. The D mixing Hamiltonian requires $(s,d) \to (c,u)$ and $V_{ts}^* V_{td} \to V_{cb}^* V_{ub}$).

In the SM only the coefficient $C^{\rm VLL}$ receives sizable contributions (in the D meson sector the GIM cancelation is more effective due to the smallness of the b quark with respect to the top one).

In the T2HDM there are no tree-level flavor changing neutral Higgs currents involving down quarks; hence the Wilson coefficients for K, B and B_s mixing receive non standard contributions only through charged Higgs box diagrams. The latter can be found, for instance, in Eq. (A.11) of Ref. [71] †.

The situation is different for what concerns $D - \bar{D}$ mixing. In fact, from Eqs. (11) and (26), it follows that the $\bar{u}_L c_R S^0$ ($S = h,\ H,\ A$) coupling is non-vanishing (albeit quite small);

†We defined the couplings $P_{LR,RL}^{H,G}$ in Eq. (10) in complete analogy to Ref. [71]

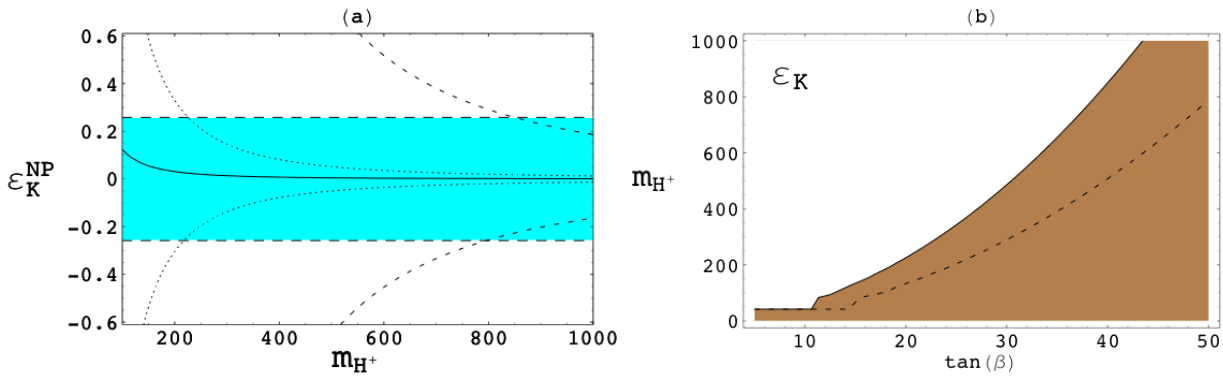

Figure 8: **Plot a**. $m_{H^\pm}$ dependence of the T2HDM contributions to ε_K in units of 10^{-3} ($\varepsilon_K^{\rm NP} \equiv \varepsilon_K^{\rm T2HDM} - \varepsilon_K^{\rm SM}$). Solid, dotted and dashed lines correspond to $|\xi| = 1$ and $\tan\beta_H = 10$, 20 and 40, respectively. Curves with $\varepsilon_K^{\rm NP}$ positive and negative correspond to $\xi = (1, -1)$, respectively. There is no appreciable dependence on ξ'. The meaning of the blue region is explained in the text. **Plot b**. Portion of the $(\tan\beta_H, m_{H^\pm})$ plane excluded by ε_K. The shaded area corresponds to $\xi = 1$. The dashed line show how this region changes for $\xi = e^{i\pi/4}$. Other choices of the phase yield in-between lines.

therefore, it induces a tree level contribution to the Wilson coefficient C_1^{SLL}. The charged Higgs box diagram contributions are obtained from Eq. (A.11) of Ref. [71] with the following replacements: $d \to u$, $P_A^B \to (P_A^B)^\dagger$ (for $A = LR, RL$ and $B = G, H$), $V \to V^\dagger$, $LR \leftrightarrow RL$ and $(ji) \to (21)$. Neutral Higgs box diagrams involve the small $\bar{u}_L c_R S^0$ coupling and are suppressed with respect to the tree level contributions.

5.2.1 $K\overline{K}$ mixing

The $K - \overline{K}$ mass difference and the measure of indirect CP violation in the K system are given by (see for instance Ref. [64])

$$\Delta m_K = 2\,{\rm Re}(M_{12}^K)\,, \tag{51}$$

$$\varepsilon_K \equiv \frac{A(K_L \to (\pi\pi)_{I=0})}{A(K_S \to (\pi\pi)_{I=0})} = \frac{\exp(i\pi/4)}{\sqrt{2}\Delta m_K}\,{\rm Im}(M_{12}^K)\,. \tag{52}$$

The expression for M_{12}^K in presence of arbitrary new physics contributions is [62, 64, 65]:

$$(M_{12}^K)^* = \frac{G_F^2}{12\pi^2} f_K^2 \hat{B}_K m_K m_W^2 \left[\lambda_c^{*2}\eta_1 S_0(x_c) + \lambda_t^{*2}\eta_2 F_{tt}^K + 2\lambda_c^*\lambda_t^*\eta_3 S_0(x_c, x_t)\right]\,, \tag{53}$$

$$\begin{aligned} F_{tt}^K &= \left[S_0(x_t) + \frac{1}{4r}C_{\rm new,K}^{VLL}\right] + \frac{1}{4r}C_{1,K}^{VRR} + \bar{P}_{1,K}^{LR}C_{1,K}^{LR} + \bar{P}_{1,K}^{LR}C_{1,K}^{LR} \\ &\quad + \bar{P}_{1,K}^{SLL}\left[C_{1,K}^{SLL} + C_{1,K}^{SRR}\right] + \bar{P}_{2,K}^{SLL}\left[C_{2,K}^{SLL} + C_{2,K}^{SRR}\right]\,, \end{aligned} \tag{54}$$

where $\lambda_i = V_{is}^* V_{id}$, $x_t = M_t^2/m_W^2$, $x_c = M_c^2/m_W^2$, the functions S_0 are given for instance in Ref. [64], η_i and r are the QCD correction to $S_0(x_t)$ in the SM, f_K is the kaon decay constant,

$\hat{B}_K$ and $\bar{P}_i^A \equiv P_i^A/(4\eta_2\hat{B}_K)$ are lattice QCD determinations of the matrix elements of the operators in Eq. (50) [62, 65]. The numerical inputs the we use are summarized in Tables 2-3.

The $K\overline{K}$ mass difference receives additional long distance contributions; in the numerical analysis we assume that such non-perturbative effects do not contribute to more than 30% of the observed mass splitting (i.e. $(\Delta m_K)_{NP} < 0.00159$ ps^{-1}). See Ref. [72] for an estimation of these long distance effects in the large N_c limit. An approximate expression for Δm_K is the following:

$$\Delta m_K \simeq \frac{G_F^2}{6\pi^2} f_K^2 \hat{B}_K m_K \mathrm{Re}(\lambda_c^{*2}) \left(\eta_1 \left[m_c(m_c)\right]^2 + \frac{\eta_2}{r} \frac{\left[m_c(m_t)\right]^4 \tan^4\beta_H}{4\, m_{H^\pm}^2} \right) . \tag{55}$$

Imposing the $(\Delta m_K)_{NP} < 0.00159$ ps^{-1} constraint, we obtain: $m_{H^\pm} > 89\ (\tan\beta_H/25)^2$ GeV.

The exact numerical impact of the upper limit on $(\Delta m_K)_{NP}$ can be seen in Fig. 7. Comparison with Fig. 5b shows that for $\xi > 0$, this constraint is complementary to $B \to X_s\gamma$.

The impact of the ε_K measurement is shown in Fig. 8. Here we require $\varepsilon_K^{\mathrm{T2HDM}}$ to lie in the ε_K range extracted from the standard unitarity triangle analysis. A more correct approach is to fit the unitarity triangle in the T2HDM and check whether each given point in the parameter space gives an acceptable chi-square. This analysis is presented in Sec. 4.

We find that the inclusion of the ε_K constraint has a very strong impact. Note that, in this case, the effect is proportional to ξ; hence, $B \to X_s\gamma$ is still required in the $\xi \sim 0$ limit.

5.2.2 $B_q\overline{B}_q$ mixing

The $B_q - \bar{B}_q$ mass difference is given by [71]

$$\Delta m_{B_q} \;=\; \frac{G_F^2 m_W^2}{6\pi^2} m_{B_q} \eta_B f_{B_q}^2 \hat{B}_{B_q} \left|V_{tb}V_{tq}^*\right|^2 \left|F_{tt}^{B_q}\right| \tag{56}$$

where $F_{tt}^{B_q}$ is given by Eq. (54) with the replacement $K \to B_q$. We recalculated the quantities $\bar{P}_i^A \equiv P_i^A/(4\eta_B\hat{B}_{B_q})$ using the formulae presented in Ref. [65] and the lattice results of Ref. [73, 74]. The numerical inputs that we use are collected in Table 4.

The SM prediction for Δm_{B_s} does not depend on the extraction of the CKM parameters ρ and η; using the inputs summarized in Table 4, we obtain $\Delta m_{B_s}^{SM} = (20.5 \pm 3.1)$ ps^{-1}. Note that, in the SM, it is possible to use the measurement of Δm_{B_d} to obtain a second determination of $f_{B_d}\sqrt{B_d}$ and of $f_{B_s}\sqrt{B_s}$ (via ξ_s), thus reducing the error on the prediction for ΔM_{B_s}.

The situation for Δm_{B_d} is different. From inspection of the standard fits of the unitarity triangle, it is clear that is always possible to choose ρ and η such that the SM prediction agrees perfectly with the experimental central value. For this reason, in the numerical, analysis we just require the new physics contributions to Δm_{B_d} to be compatible with the experimental determination up to an uncertainty given by the lattice errors on $f_{B_d}\sqrt{B_d}$. A more correct analysis requires a simultaneous fit of the new physics contributions to ε_K, Δm_{B_q}, $a_{\psi K_s}$ and $|V_{ub}/V_{cb}|$. See Ref. [75] for a general discussion of New Physics effects on B_s mixing.

From the plots in Fig. 9 we see that $B_q - \bar{B}_q$ mixing data constraints are still much weaker than the corresponding constraint on ε_K.

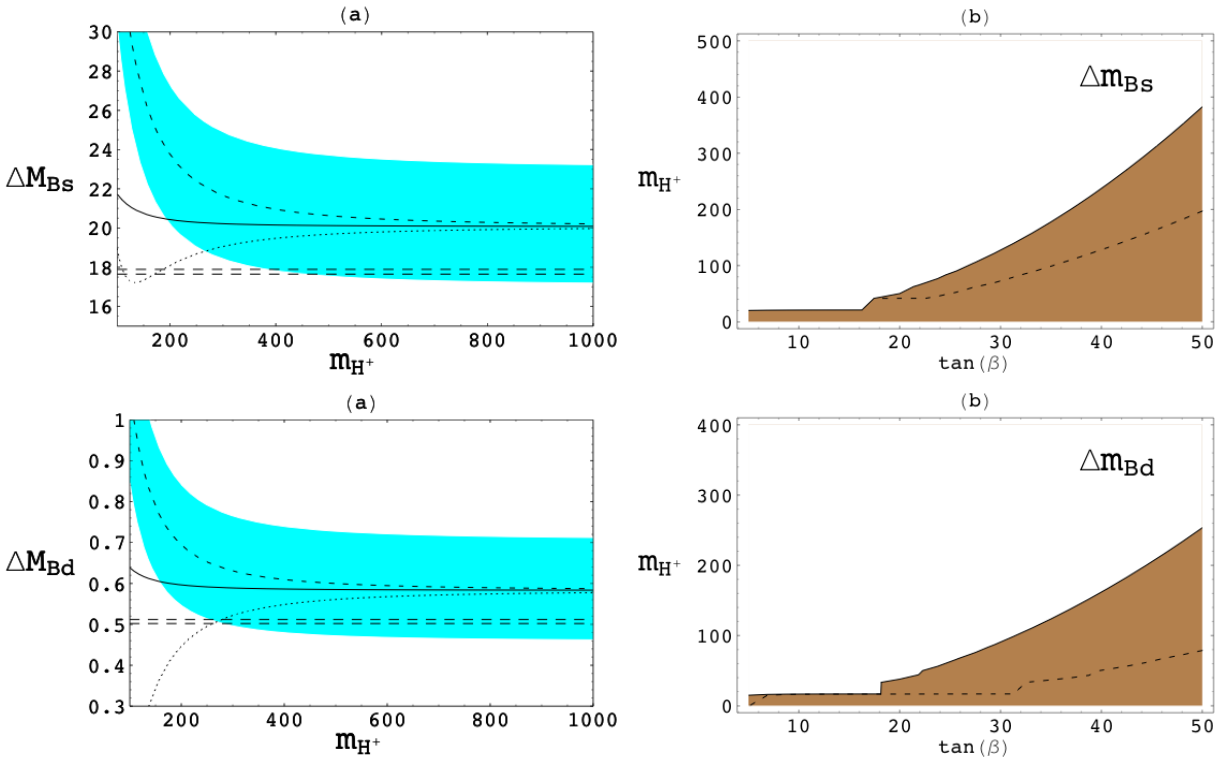

Figure 9: **Plots a**. $m_{H^\pm}$ dependence of the T2HDM contributions to $\Delta m_{B_{(s,d)}}$ in ps^{-1}. Solid, dotted and dashed lines correspond to $|\xi| = 1$ and $(\tan\beta_H, \varphi_\xi) = (30, 0)$, $(50, 0)$, $(50, \pi/2)$, respectively. There is no appreciable dependence on ξ'. The horizontal dashed lines are the experimental measurement. The blue band shows the theoretical uncertainties for the dashed line, similar bands can be drawn for the other curves. **Plots b**. Portions of the $(\tan\beta_H, m_{H^\pm})$ plane excluded by $\Delta m_{B_{(s,d)}}$. The shaded area corresponds to $\xi = 1$. The dashed line show how this region changes for $\xi = e^{i\pi/2}$. Other choices of the phase yield in-between lines.

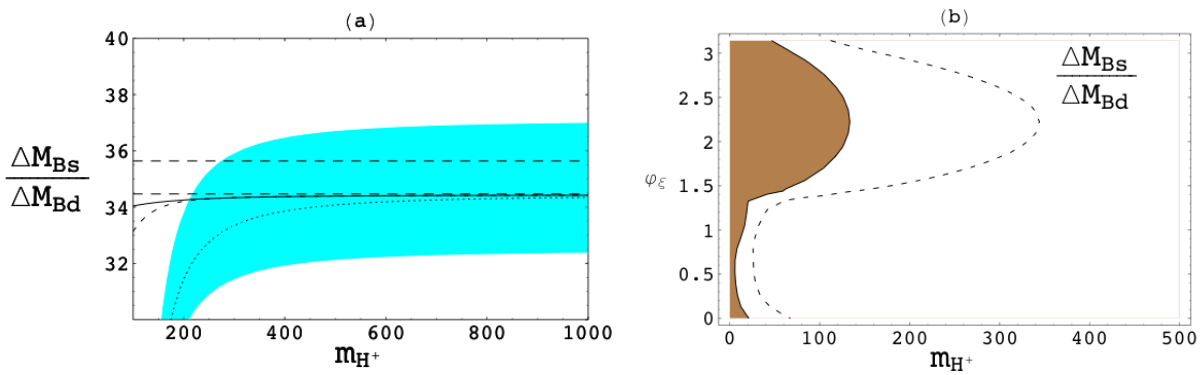

Figure 10: **Plot a**. $m_{H^\pm}$ dependence of the T2HDM contributions to $\Delta m_{B_{(s)}}/\Delta m_{B_{(d)}}$. See the caption in Fig. 9. **Plot b**. Excluded region in the $(\varphi_\xi, m_{H^\pm})$ plane. The solid and dashed contours correspond to $\tan\beta_H$ =30 and 50, respectively.

5.2.3 $D\overline{D}$ mixing

The SM prediction for δm_D range between 10^{-6} ps^{-1} and 10^{-2} ps^{-1} and is completely dominated by long distance effects; in fact, the short-distance SM prediction has been calculated and reads [76, 77] $x_D \simeq 1.5 \times 10^{-6}$ ps^{-1}. The present experimental information on $D\bar{D}$ mixing parameters [78, 79], yields the following model independent determination of the $D\bar{D}$ mass difference [80]: $\Delta m_D = (14.5 \pm 5.6)10^{-3}$ps^{-1}. In the T2HDM very large effects are possible (of order 1% [8]), and there is the possibility that the actual $D - \bar{D}$ mass difference is entirely controlled by new physics short distance effects. In the numerics we require the new physics contribution to the Δm_D not to exceed the measurement.

The $D - \bar{D}$ mass difference is given by

$$\Delta m_D = \frac{G_F^2 m_W^2}{16\pi^2 m_D} \left|V_{ub}V_{cq}^*\right|^2 \Big[(C_{1,D}^{VLL} + C_{1,D}^{VRR}) \langle Q^{VLL}\rangle + (C_{1,D}^{SLL} + C_{1,D}^{SRR}) \langle Q_1^{SLL}\rangle + (C_{2,D}^{SLL} + C_{2,D}^{SRR}) \langle Q_2^{SLL}\rangle + C_{1,D}^{LR} \langle Q_1^{LR}\rangle + C_{2,D}^{LR} \langle Q_2^{LR}\rangle \Big] \quad (57)$$

where the matrix elements are

$$\langle D|Q^{VLL}|\bar{D}\rangle = \frac{2}{3}\, m_D^2 f_D^2 \hat{B}^{VLL} \quad (58)$$

$$\langle D|Q_1^{SLL}|\bar{D}\rangle = -\frac{5}{12} R\, m_D^2 f_D^2 \hat{B}_1^{SLL} \quad (59)$$

$$\langle D|Q_2^{SLL}|\bar{D}\rangle = -R\, m_D^2 f_D^2 \hat{B}_2^{SLL} \quad (60)$$

$$\langle D|Q_1^{LR}|\bar{D}\rangle = -\frac{1}{3} R\, m_D^2 f_D^2 \hat{B}_1^{LR} \quad (61)$$

$$\langle D|Q_2^{LR}|\bar{D}\rangle = \frac{1}{2} R\, m_D^2 f_D^2 \hat{B}_2^{LR} \quad (62)$$

and $R = (m_D/(m_c + m_u))^2$. In the numerical analysis we use $\hat{B}^{VLL} = \hat{B}_D = 0.82 \pm 0.01$ [76]

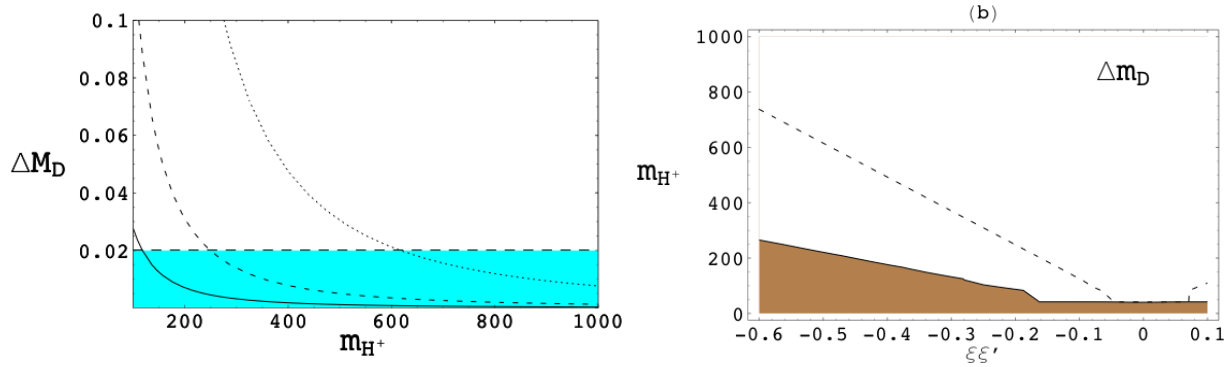

Figure 11: **Plot a**. $m_{H^\pm}$ dependence of the T2HDM contributions to Δm_D. Solid, dashed and dotted lines correspond to $|\xi\xi'| = 0.1$, 0.2 and 0.5, respectively. We fix $\tan\beta_H = 50$. The horizontal dashed line is the experimental upper limit. **Plot b**. Portion of the $(\xi\xi', m_{H^\pm})$ plane excluded by Δm_D. The shaded area corresponds to $\tan\beta_H = 30$. The dashed line to $\tan\beta_H = 50$.

(this value of the *hat* parameter $\hat{B}_D$ has been obtained from the lattice determination of $B_D(2\text{GeV})$ [69, 70]) and set all the other B parameters to 1.

An approximate expression for the $D - \bar{D}$ mass difference is given by [8]

$$\Delta m_D = \frac{G_F^2}{6\pi^2}(\xi\xi'^*)^2 \frac{m_c^4 \tan^4\beta_H}{4m_{H^\pm}^2} \,. \tag{63}$$

The strong ξ' dependence implies that, once $B \to \tau\nu$ data are imposed, no large deviations can be observed on Δm_D as can be seen from Fig 11.

5.3 $B^+ \to \tau^+\nu_\tau$

The branching ratio for the decay $B \to \tau\nu_\tau$ has been recently measured by the Belle [81] and Babar [82] collaborations

$$\mathcal{B}(B \to \tau\nu_\tau) = \left(1.79^{+0.56}_{-0.49}(\text{stat})^{+0.39}_{-0.46}(\text{syst})\right) \times 10^{-4} \;\; [\text{Belle}] \tag{64}$$

$$\mathcal{B}(B \to \tau\nu_\tau) = \left(0.88^{+0.68}_{-0.67}(\text{stat}) \pm 0.11(\text{syst})\right) \times 10^{-4} \;\; [\text{Babar}] \,, \tag{65}$$

yielding the following world average

$$\mathcal{B}_{WA}(B \to \tau\nu_\tau) = (1.31 \pm 0.48) \times 10^{-4} \,. \tag{66}$$

The SM expectation reads:

$$\mathcal{B}_{\text{SM}}(B \to \tau\nu_\tau) = \frac{G_F^2 m_B m_\tau^2}{8\pi}\left(1 - \frac{m_\tau^2}{m_B^2}\right) f_B^2 |V_{ub}|^2 \tau_B = (1.53 \pm 0.38) \times 10^{-4} \,, \tag{67}$$

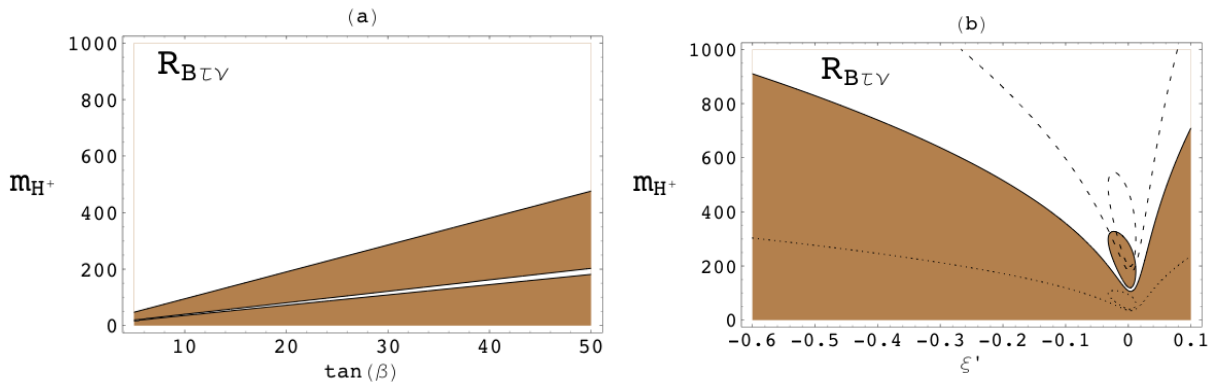

Figure 12: **Plot a**. Portion of the $(\tan\beta_H, m_{H^\pm})$ plane allowed by $R_{B\tau\nu}$ for $\xi' = 0$. **Plot b**. Excluded region in the $(\xi', m_{H^\pm})$ plane. The dotted, solid and dashed contours correspond to $\tan\beta_H$ =10, 30 and 50, respectively.

where we used the PDG world average $|V_{ub}| = (4.31 \pm 0.3) \times 10^{-3}$ from direct tree level measurements only. The above result leads to

$$R_{B\tau\nu} \;=\; \frac{\mathcal{B}_{WA}(B \to \tau\nu_\tau)}{\mathcal{B}_{\rm SM}(B \to \tau\nu_\tau)} = 0.86 \pm 0.38\,. \tag{68}$$

If we use the fitted value of the CKM angles ($|V_{ub}| = (3.68 \pm 0.14) \times 10^{-3}$, the prediction reads $R_{B\tau\nu} = 1.18 \pm 0.50$. The discrepancy between this determination of $R_{B\tau\nu}$ and Eq. (68) is a manifestation of the conflict within the SM between the present determinations of V_{ub} and $\sin(2\beta)$.

In the T2HDM this process receives large tree level contributions via charged Higgs exchange:

$$\mathcal{B}(B \to \tau\nu_\tau) \;=\; \mathcal{B}_{\rm SM}(B \to \tau\nu_\tau)\left|1 - \tan^2\beta_H \frac{m_B^2}{m_{H^\pm}^2}\left(1 - \frac{(\Sigma^\dagger V)_{13}}{m_b V_{ub}}\right)\right|^2 \tag{69}$$

$$\simeq\; \mathcal{B}_{\rm SM}(B \to \tau\nu_\tau)\left|1 - \tan^2\beta_H \frac{m_B^2}{m_{H^\pm}^2}\left(1 - \xi'^{*}\frac{m_c V_{tb}}{m_b V_{ub}}\right)\right|^2 . \tag{70}$$

The numerical impact of the constraint in Eq. (68) is very strong. In Fig. 12b we show the impact of this constraint onto the $(\xi', m_{H^\pm})$ plane for various values of $\tan\beta_H$. Since the experimental to SM ratio in Eq. (68) is smaller than 1, scenarios with $\xi' > 0$ are disfavored (see Eq. (70)).

5.4 Time-dependent CP asymmetry in $B \to (J/\psi, \phi, \eta')\, K_s$

The time dependent CP asymmetry in the decay $B \to fK_s$ ($f = J/\psi, \phi, \eta'$) is given by

$$a_{fK} \;=\; \frac{2\,{\rm Im}\lambda_{fK}}{1 + |\lambda_{fK}|^2} \tag{71}$$

$$\lambda_{\psi K} \;=\; -\frac{(M_{12}^{B_d})^*}{|M_{12}^{B_d}|}\frac{A(\bar{B}^0 \to fK_s)}{A(B^0 \to fK_s)} = -e^{-2i\beta}\frac{F_{tt}^{B_d}}{|F_{tt}^{B_d}|}\frac{A(\bar{B}^0 \to fK_s)}{A(B^0 \to fK_s)}\,, \tag{72}$$

where $F_{tt}^{B_d}$ is obtained from Eq. (54) with obvious replacements. The effective Hamiltonian that controls the amplitude $A(\bar{B}^0 \to f K_s)$ in the T2HDM is [50]:

$$\mathcal{H}_{eff} = -\frac{4G_F}{\sqrt{2}} V_{ts}^* V_{tb} \left[\sum_{i=1}^{6} C_i(\mu) O_i(\mu) + \sum_{i=3}^{6} C_{iQ}(\mu) O_{iQ}(\mu) + C_R(\mu)\, O_R(\mu) \right] , \tag{73}$$

where

$$\begin{aligned}
O_1 &= (\bar{s}_L \gamma_\mu T^a c_L)(\bar{c}_L \gamma^\mu T^a b_L), && (74)\\
O_2 &= (\bar{s}_L \gamma_\mu c_L)(\bar{c}_L \gamma^\mu b_L), && (75)\\
O_3 &= (\bar{s}_L \gamma_\mu b_L) \sum (\bar{q} \gamma^\mu q), && (76)\\
O_4 &= (\bar{s}_L \gamma_\mu T^a b_L) \sum (\bar{q} \gamma^\mu T^a q), && (77)\\
O_5 &= (\bar{s}_L \gamma_{\mu_1} \gamma_{\mu_2} \gamma_{\mu_3} b_L) \sum (\bar{q} \gamma^{\mu_1} \gamma^{\mu_2} \gamma^{\mu_3} q), && (78)\\
O_6 &= (\bar{s}_L \gamma_{\mu_1} \gamma_{\mu_2} \gamma_{\mu_3} T^a b_L) \sum (\bar{q} \gamma^{\mu_1} \gamma^{\mu_2} \gamma^{\mu_3} T^a q), && (79)\\
O_{3Q} &= (\bar{s}_L \gamma_\mu b_L) \sum Q_q (\bar{q} \gamma^\mu q), && (80)\\
O_{4Q} &= (\bar{s}_L \gamma_\mu T^a b_L) \sum Q_q (\bar{q} \gamma^\mu T^a q), && (81)\\
O_{5Q} &= (\bar{s}_L \gamma_{\mu_1} \gamma_{\mu_2} \gamma_{\mu_3} b_L) \sum Q_q (\bar{q} \gamma^{\mu_1} \gamma^{\mu_2} \gamma^{\mu_3} q), && (82)\\
O_{6Q} &= (\bar{s}_L \gamma_{\mu_1} \gamma_{\mu_2} \gamma_{\mu_3} T^a b_L) \sum Q_q (\bar{q} \gamma^{\mu_1} \gamma^{\mu_2} \gamma^{\mu_3} T^a q), && (83)\\
O_R &= (\bar{c}_R b_L)\, (\bar{s}_L c_R). && (84)
\end{aligned}$$

Tree level and one–loop charged Higgs diagrams contribute to the following matching conditions (we adopt the notation of Ref. [50]):

$$\begin{aligned}
C_R^{(00)}(\mu_0) &= -\frac{\left(4 V_{cb} V_{cs}^* G_F/\sqrt{2}\right)^{-1}}{m_{H^\pm}^2} (P_{RL}^H)_{23}\, (P_{RL}^H)_{22}^* \simeq \frac{V_{tb}}{V_{cb}} \frac{m_c^2}{m_{H^\pm}^2} \xi^* \tan^2\beta_H \ , && (85)\\
\delta C_4^{(10)}(\mu_0) &= E_H(x_{th}) \frac{\kappa}{\tan^2\beta_H} \ , && (86)\\
\delta C_3^{(11)}(\mu_0) &= -\frac{2}{9 s_W^2} C_H(x_{th}) \frac{\kappa}{\tan^2\beta_H} && (87)\\
\delta C_5^{(11)}(\mu_0) &= -\frac{1}{4} \delta C_3^{(11)}(\mu_0) \ , && (88)\\
\delta C_{3Q}^{(11)}(\mu_0) &= \left[D_H(x_{th}) + 4\, C_H(x_{th}) \left(1 + \frac{1}{3 s_W^2} \right) \right] \frac{\kappa}{\tan^2\beta_H} \ , && (89)\\
\delta C_{5Q}^{(11)}(\mu_0) &= \frac{3}{2} \delta C_3^{(11)}(\mu_0) \ , && (90)
\end{aligned}$$

where $\mu_0 \sim O(m_t)$, $x_{th} = m_t^2/m_{H^\pm}^2$ and

$$\kappa = \frac{(P_{RL}^H)_{33}\, (P_{RL}^H)_{32}^*\, \tan^2\beta_H}{V_{tb} V_{ts}^*\, m_t^2\, 4G_F/\sqrt{2}} \simeq 1 - \xi^* \tan^2\beta_H \frac{V_{cs}^*}{V_{ts}^*} \left(\frac{m_c}{m_t}\right)^2 \simeq 1 - 0.3\, \xi^* \left(\frac{\tan\beta_H}{30}\right)^2 \tag{91}$$

The functions E_H, D_H and C_H can be found in Appendix A of Ref. [83]. Note that the results for the type-II 2HDM are recovered in the $\kappa \to 1$ limit.

Direct calculation of the anomalous dimensions involving the operator O_R yields (in the notation of Ref. [50]):

$$\gamma_{RR}^{(10)} = -16 \,, \tag{92}$$

$$\gamma_{R4}^{(10)} = -\frac{2}{3} \,, \tag{93}$$

$$\gamma_{Rj}^{(10)} = 0 \ (\mathrm{j} \neq \mathrm{R}, 4) \,. \tag{94}$$

$$\tag{95}$$

The large anomalous dimension of O_R implies a large impact of the running from the high-scale $\mu_0 \sim O(m_t)$ to the low-scale $\mu_b \sim O(m_b)$:

$$C_R(\mu_b) = \eta^{-1.04348} \, C_R(\mu_0) \,, \tag{96}$$

where $\eta = \alpha_s(\mu_0)/\alpha_s(\mu_b) \simeq 0.53$.

Let us first consider $A(\bar{B}^0 \to J/\psi K_s)$. The impact of the QCD and electroweak penguin coefficients is very small; hence the only T2HDM effect comes via the new operator O_R. Adopting the naive factorization framework, the amplitude is proportional to:

$$\begin{aligned} A(\bar{B}^0 \to J/\psi K_s) \propto\ & \frac{4}{9} C_1(\mu_b) + \frac{1}{3} C_2(\mu_b) + 2\, C_3(\mu_b) + 20\, C_5(\mu_b) + \frac{4}{3} C_{3Q}(\mu_b) + \frac{40}{3} C_{5Q}(\mu_b) \\ & - \frac{1}{6} C_R(\mu_b) \,, \end{aligned} \tag{97}$$

where the C_R contribution receives a factor of $-1/2$ and $1/3$ from Lorentz and color Fierzing, respectively. Note that the SM contribution (see for instance Ref. [84]) has been rewritten in the new operator basis Eq. (73). Direct calculation of this amplitude in the QCD–factorization approach [84] shows that the naive estimate is a fairly good approximation.

The analysis of the amplitudes $A(\bar{B}^0 \to (\phi, \eta') K_s)$ is more complicated. In this case the QCD and electroweak penguin coefficients do play a leading role; moreover the magnetic penguin operator O_8 contributes as well. In the following we adopt the QCD-factorization analysis presented in Ref. [85]. After transforming the Wilson coefficients of Ref. [85] into our basis, we obtain the following expressions for the ϕ and η' amplitudes:

$$\begin{aligned} A(\bar{B}^0 \to \eta' K_s) \propto\ & (-0.04874 - 0.04905i) - (0.00658 - 0.00058i)\, \delta C_3^{(11)}(\mu_0) \\ & -(0.00014 - 0.00002i)\, \delta C_{3Q}^{(11)}(\mu_0) + (0.00711 - 0.00275i)\, \delta C_4^{(10)}(\mu_0) \\ & +0.0007\, C_7(\mu_b) - 0.089\, C_8(\mu_b) + (0.03567 - 0.01087i)\, C_R(\mu_0) \,, \end{aligned} \tag{98}$$

$$\begin{aligned} A(\bar{B}^0 \to \phi K_s) \propto\ & (0.03262 + 0.00791i) + (0.00963 - 0.00050i)\, \delta C_3^{(11)}(\mu_0) \\ & +(0.00044 - 0.00002i)\, \delta C_{3Q}^{(11)}(\mu_0) - (0.00282 - 0.00013i)\, \delta C_4^{(10)}(\mu_0) \\ & -0.0004\, C_7(\mu_b) + 0.047\, C_8(\mu_b) - (0.01292 - 0.00092i)\, C_R(\mu_0) \,. \end{aligned} \tag{99}$$

Note that the impact of the QCD and electroweak penguin matching conditions is suppressed by an order of magnitude with the respect to the leading contribution; in fact, the low–scale penguin Wilson coefficients are dominated by the tree-level coefficient C_2 via the RGE running. Not surprisingly, the effect of the other tree-level operator (O_R) on the running is also very large.

The experimental measurements of these three asymmetries read [14]:

$$a_{\psi K} = 0.675 \pm 0.026 \,, \tag{100}$$
$$a_{\eta' K} = 0.61 \pm 0.07 \,, \tag{101}$$
$$a_{\phi K} = 0.39 \pm 0.18 \,. \tag{102}$$
$$\tag{103}$$

In Fig. 13a, we show the size of T2HDM contributions to the CP asymmetries in $B \to (J/\psi, \eta', \phi) K_S$ for some choice of input parameters. In Fig. 13b, we show the portion of the $(\tan\beta_H, m_{H^\pm})$ parameter space that is allowed by the present measurements of these asymmetries. From the inspection of the figures we see that at the 1σ level it is possible to reconcile the $B \to \psi$ and $B \to \eta'$ asymmetries in a quite wide region of the parameter space. The $B \to \phi$ asymmetry, on the other hand, requires a too light charged Higgs.

5.5 $\Delta\Gamma_s/\Gamma_s$

The B_s-$\bar{B}_s$ width difference is given by

$$\Delta\Gamma_s = -2\,\Gamma_{12}^s \cos(\beta_s + \theta_s) = -2\Big([\Gamma_{12}^s]_{SM} + \delta\Gamma_{12}^s\Big)\cos(\beta_s + \theta_s) \tag{104}$$
$$\Gamma_{12}^s = \frac{1}{2m_{B_s}} \langle \bar{B}_s | \mathrm{Im}\left\{ i \int d^4x \; T \; \mathcal{H}_{\rm eff}(x) \mathcal{H}_{\rm eff}(0) \right\} | B_s \rangle \tag{105}$$

where, in the Standard Model, $\mathcal{H}_{\rm eff}$ is the effective Hamiltonian that mediates the bottom quark decay and is dominated by tree level contributions. T2HDM contributions affect both θ_s and Γ_{12}^s: the former has been already discussed in Sec. 5.2.2; the latter are induced by a new $\Delta B = 1$ operator. The structure of the charged Higgs couplings in Eqs. (15) and (16), implies that the operator O_R receives the largest contributions. In the numerics we will consider its effects together with the interference with the dominant Standard Model operator O_2 (see Eq. (73) for the definition of the operators).

Direct calculation of the T-product in Eq. (105) yields the following leading order expression for the new physics contribution to Γ_{12}^s:

$$\delta\Delta\Gamma_{12}^s = -\frac{G_F^2 m_{b,pole}^2}{12\pi(2m_{B_s})} (V_{cb}^* V_{cs})^2 \sqrt{1-4z_c} \Bigg[\left(\frac{1-4z_c}{2} \frac{C_{RR}^2}{4} + \frac{C_2 C_{RR}}{2} M_{c,pole}^2 M_{b,pole}^2 \right) \langle Q \rangle - (1+2z_c) \frac{C_{RR}^2}{4} \langle Q_S \rangle \Bigg] \tag{106}$$

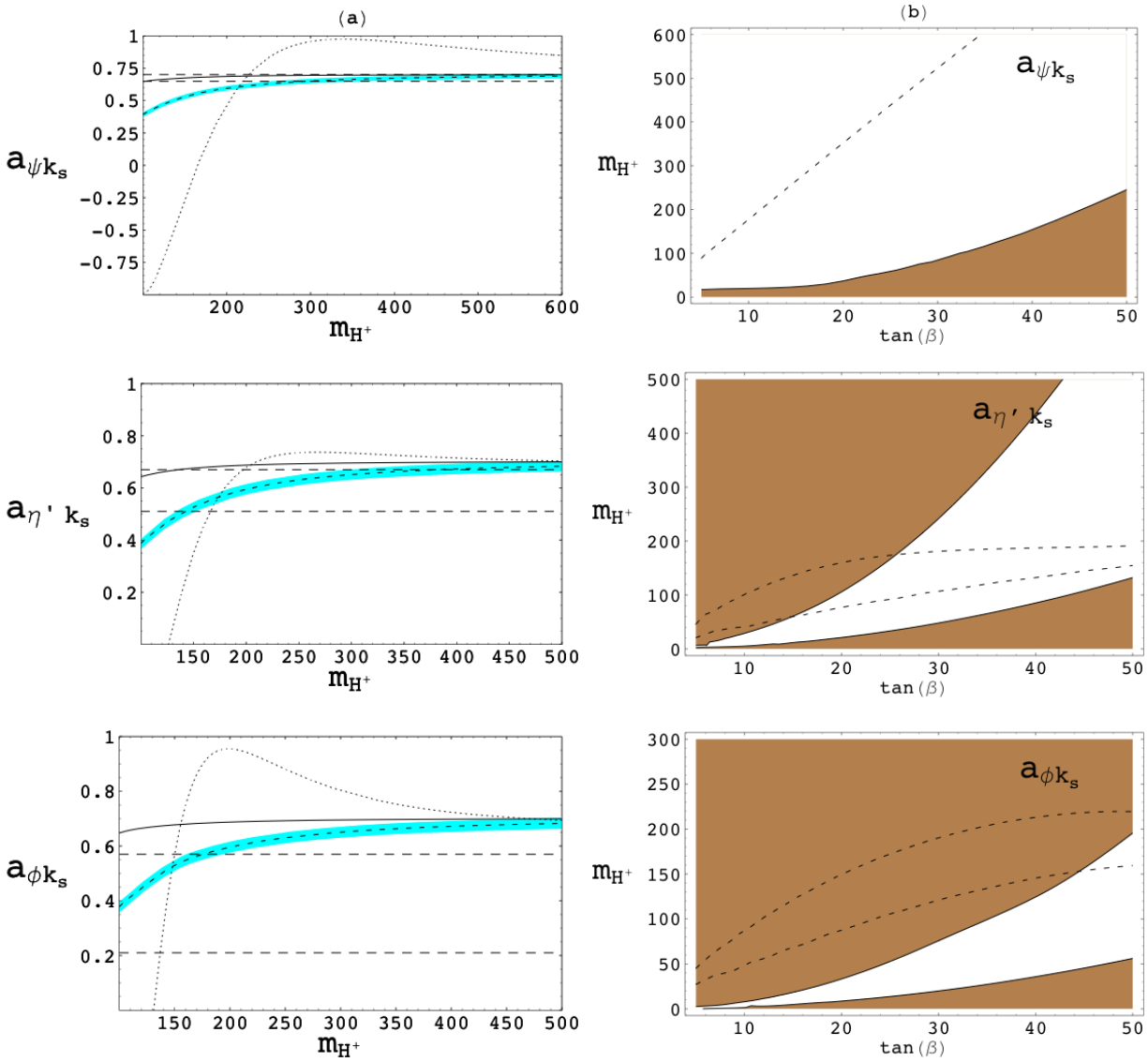

Figure 13: **Plot a**. $m_{H^\pm}$ dependence of the T2HDM contributions to $a_{(\psi,\eta',\phi)K}$. Solid, dotted and dashed lines correspond to $|\xi| = 1$ and $(\tan\beta_H, \varphi_\xi) = (30, 0)$, $(50, 0)$, $(50, \pi/2)$, respectively. There is no appreciable dependence on ξ'. The horizontal dashed lines are the experimental measurement. The blue band shows the theoretical uncertainties. **Plot b**. Portion of the $(\tan\beta_H, m_{H^\pm})$ plane excluded by $a_{(\psi,\eta',\phi)K}$. The shaded area corresponds to $\xi = 1$. The dashed line show how this region changes for $\xi = e^{i\pi/2}$ (in the first plot, the region excluded is below the dashed line; in the second and third plots, it is above the uppermost dashed line and below the lowermost one). Other choices of the phase yield in-between contours.

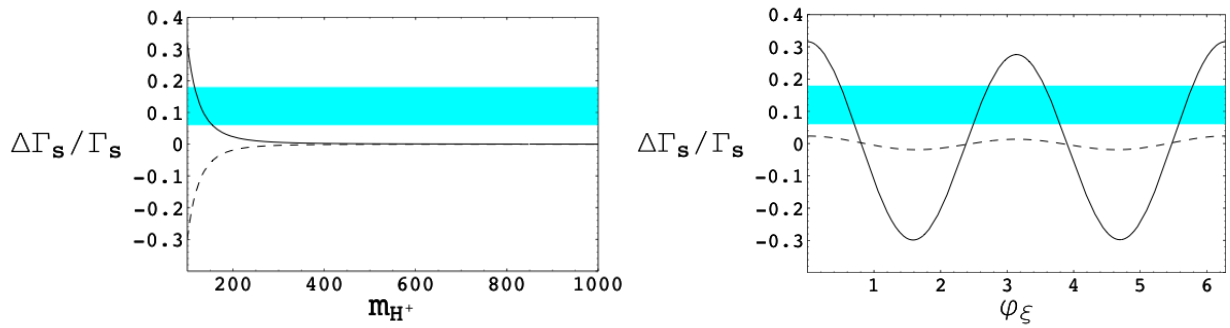

Figure 14: **Plot a**. $m_{H^\pm}$ dependence of the T2HDM contributions to $\Delta\Gamma_s/\Gamma_s$. We take $|\xi| = 1$ and $\tan\beta_H = 50$. Solid and dashed lines correspond to $\varphi_\xi = 0$ and $\pi/2$, respectively. The blue band is the experimental 68% C.L. allowed region. **Plot b**. φ_ξ dependence of the T2HDM contributions to $\Delta\Gamma_s/\Gamma_s$. We take $|\xi| = 1$ and $\tan\beta_H = 50$. Solid and dashed lines correspond to $m_{H^\pm} = 100$ and 200, respectively.

where the operators Q and Q_S are

$$Q = (\bar{b}s)_{V-A}(\bar{b}s)_{V-A} \ , \tag{107}$$

$$Q_S = (\bar{b}s)_{S-P}(\bar{b}s)_{S-P} \tag{108}$$

and their matrix elements between $\bar{B}_s$ and B_s states are

$$\langle Q \rangle = f_{Bs}^2 m_{B_s}^2 \left(1 + \frac{1}{N_c}\right) B \ , \tag{109}$$

$$\langle Q_S \rangle = -f_{Bs}^2 m_{B_s}^2 \frac{m_{B_s}^2}{(m_b + m_s)^2} \left(2 - \frac{1}{N_c}\right) B_S \ , \tag{110}$$

with $B = 0.87 \pm 0.06$ and $B_S = 0.84 \pm 0.05$ [86]. After normalizing to the total B_s width we obtain:

$$\frac{\Delta\Gamma_s}{\Gamma_s} = \tau_{B_s}\Delta\Gamma_s = \left[\frac{\Delta\Gamma_s}{\Gamma_s}\right]_{\rm SM} + \tau_{B_s}\ \delta\Delta\Gamma_s \cos(\beta_s + \theta_s) \ . \tag{111}$$

The SM prediction [87, 88] and the experimental result [25, 89] read:

$$\left[\frac{\Delta\Gamma_s}{\Gamma_s}\right]_{\rm SM} = 0.147 \pm 0.060 \ , \tag{112}$$

$$\left[\frac{\Delta\Gamma_s}{\Gamma_s}\right]_{\rm exp} = 0.27 \pm 0.08 \ . \tag{113}$$

5.6 CP asymmetry in flavor specific B decays

The CP asymmetry in flavor specific B_q decays (only the decays $B_q \to f$ and $\bar{B}_q \to \bar{f}$ are allowed) is given by:

$$A_{SL}^{(q)} \equiv \frac{\Gamma(\bar{B}_q(t) \to f) - \Gamma(B_q(t) \to \bar{f})}{\Gamma(\bar{B}_q(t) \to f) + \Gamma(B_q(t) \to \bar{f})} = \mathrm{Im}\frac{\Gamma_{12}^{(q)}}{M_{12}^{(q)}} \ . \tag{114}$$

From the discussion in Sec. 5.5 it follows that the T2HDM effects on $\Gamma_{12}^{(q)}$ are negligible, hence we will consider only box diagram contributions to $M_{12}^{(q)}$. Adopting the standard parametrization, $M_{12}^{(q)}/M_{12,SM}^{(q)} = r_q^2 \exp(2i\theta_q)$ we get:

$$A_{SL}^{(q)} = \mathrm{Im}\left(\frac{\Gamma_{12}^{(q)}}{M_{12}^{(q)}}\right)_{\mathrm{SM}} \frac{\cos 2\theta_q}{r_q^2} - \mathrm{Re}\left(\frac{\Gamma_{12}^{(q)}}{M_{12}^{(q)}}\right)_{\mathrm{SM}} \frac{\sin 2\theta_q}{r_q^2} \ , \tag{115}$$

where [86, 90]

$$\left(\Gamma_{12}^{(d)}/M_{12}^{(d)}\right)_{\mathrm{SM}} = \Big[-(40 \pm 16) - i\,(5 \pm 1)\Big] \times 10^{-4} \tag{116}$$

$$\left(\Gamma_{12}^{(s)}/M_{12}^{(s)}\right)_{\mathrm{SM}} = \Big[-(40 \pm 16) + i\,(0.22 \pm 0.04)\Big] \times 10^{-4} \ . \tag{117}$$

In the notation of Sec. 5.2.2, we have $r_q^2 \ \exp(2i\theta_q) = F_{tt}^{B_q}/S_0(x_t)$. From Eqs. (116,117) we read the SM predictions:

$$\left(A_{SL}^{(d)}\right)_{\mathrm{SM}} = (5 \pm 1) \times 10^{-4} \tag{118}$$

$$\left(A_{SL}^{(d)}\right)_{\mathrm{SM}} = (0.22 \pm 0.04) \times 10^{-4} \ . \tag{119}$$

Unfortunately the experimental errors on these asymmetries are at least an order of magnitude larger than the SM expectations [91–96]:

$$\left(A_{SL}^{(d)}\right)_{\mathrm{exp}} = (11 \pm 55) \times 10^{-4} \tag{120}$$

$$\left(A_{SL}^{(s)}\right)_{\mathrm{exp}} = (-80 \pm 110) \times 10^{-4} \ . \tag{121}$$

In Fig. 15 we show the size of the T2HDM contributions to these asymmetries for large $\tan\beta_H$.

5.7 Neutron EDM

The effective Hamiltonian that encodes charged Higgs contributions to the neutron EDM is:

$$\mathcal{H}_{\mathrm{eff}} = \sum_{q=u,d} C_q \left[\frac{e}{16\pi^2}(\bar{q}_L \sigma^{\mu\nu} q_R) F_{\mu\nu} \ ,\right] \tag{122}$$

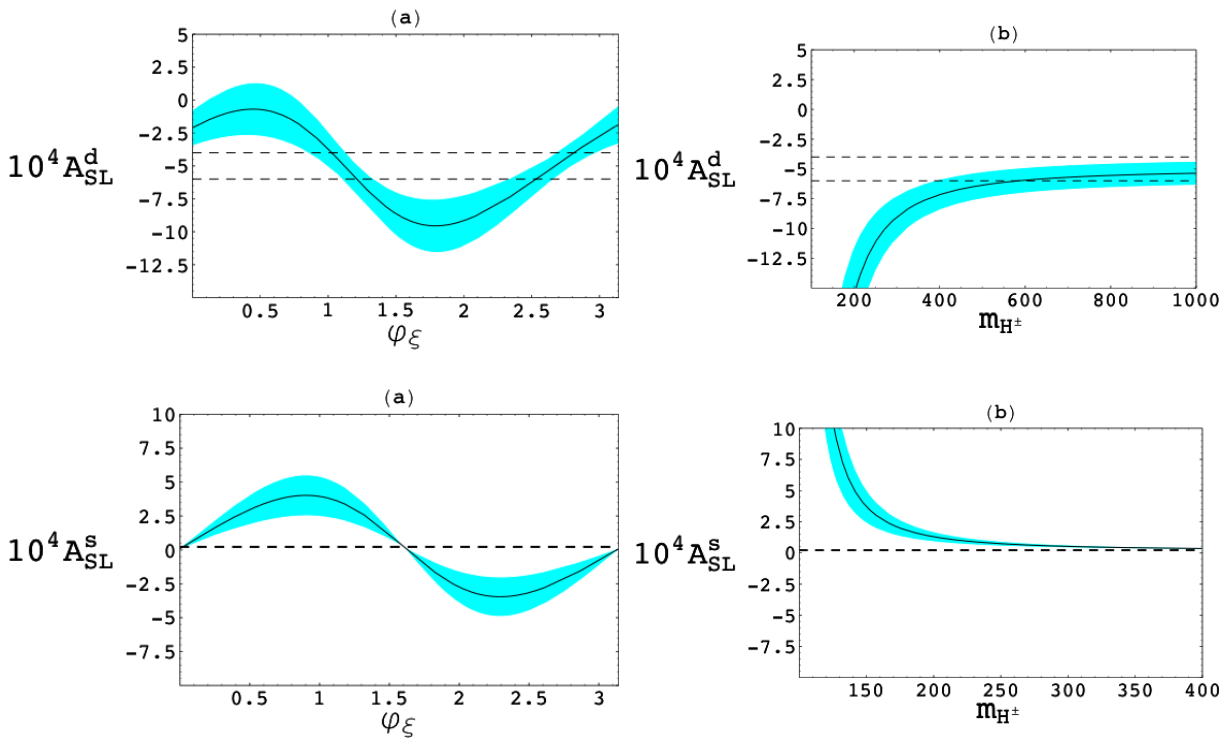

Figure 15: φ_ξ and $m_{H^\pm}$ dependence of $A_{SL}^{(d,s)}$ for $|\xi| = 1$ and $\tan\beta_H = 50$. The dashed lines are the 1σ SM expectation. The blue band is the theoretical error.

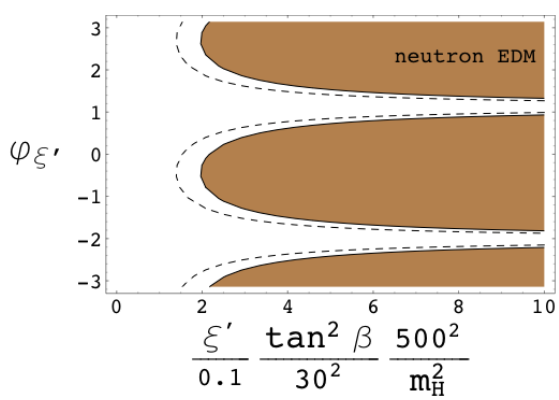

Figure 16: Constraint that the neutron EDM puts on the T2HDM parameter space. The shaded area is excluded at 90% CL. The solid and dashed lines correspond to $m_{H^\pm} = (200, 1000)$ GeV.

where

$$C_d = \sum_{i=1}^{3} \left\{ \frac{(P^H_{LR})_{i1}(P^H_{RL})^*_{i1}}{m_{u_i}} B\left(\frac{m^2_{u_i}}{m^2_{H^\pm}}\right) + \cdots \right\} , \tag{123}$$

$$C_u = \sum_{i=1}^{3} \left\{ \frac{(P^H_{LR})_{1i}(P^H_{RL})^*_{1i}}{m_{d_i}} B\left(\frac{m^2_{d_i}}{m^2_{H^\pm}}\right) + \cdots \right\} , \tag{124}$$

and the function B is given in Ref. [36]. The dots stand for terms that do not contribute to the imaginary part of the Wilson coefficients. In the chiral quark model, the neutron EDM is related the valence quark EDM's, d_u and d_d, via [97]:

$$d_n = \frac{1}{3}\left(4\, d_d - d_u\right)\, \eta^E , \tag{125}$$

$$d_q = \frac{e}{16\pi^2}\, \mathrm{Im}(C_q) , \tag{126}$$

where $\eta^E \simeq 1.53$ is the QCD correction factor. Approximate formulae for the up and down quark contributions to the neutron EDM are (in units of e cm):

$$\frac{4}{3}\eta^E d_d = 10^{-29}\, \xi \left(\frac{\tan\beta_H}{30}\right)^2 \left(\frac{500}{m_{H^\pm}}\right)^2 \left[-(6.5 \pm 0.3)\cos\varphi_\xi - (15.9 \pm 0.7)\sin\varphi_\xi\right] \tag{127}$$

$$-\frac{1}{3}\eta^E d_u = 10^{-26}\, \frac{\xi'}{0.1} \left(\frac{\tan\beta_H}{30}\right)^2 \left(\frac{500}{m_{H^\pm}}\right)^2 \left[(3.5 \pm 0.6)\cos\varphi_{\xi'} - (1.65 \pm 0.3)\sin\varphi_{\xi'}\right] \tag{128}$$

where the uncertainties come from varying $m_{H^\pm}$ in the $(200 - 1000)$ GeV range. Taking into account that the 90% C.L. experimental upper bound on the neutron EDM is [25] 6.3×10^{-26} e cm, it is clear that the T2HDM parameter space is constrained only for $\xi' \neq 0$. Note that the huge enhancement in d_u comes from $\Sigma_{13} \propto m_c \tan\beta_H \xi'/m_W$ that is not suppressed either by V_{ub} or, for large $\tan\beta_H$, by the charm Yukawa.

In Fig. 16 we show the impact of the present upper bound on the T2HDM parameter space.

5.8 CP asymmetries in $B^- \to K^-\pi^0$ and $\bar{B}^0 \to K^-\pi^+$

The direct CP asymmetries in the decays $B^- \to K^-\pi^0$ and $\bar{B}^0 \to K^-\pi^+$ can be calculated (albeit with large errors) in the QCD factorization approach [31]:

$$A_{CP}(B^- \to K^-\pi^0) = \left(7.1^{+1.7+2.0+0.8+9.0}_{-1.8-2.0-0.6-9.7}\right)\% \tag{129}$$

$$A_{CP}(\bar{B}^0 \to K^-\pi^+) = \left(4.5^{+1.1+2.2+0.5+8.7}_{-1.1-2.5-0.6-9.5}\right)\% , \tag{130}$$

where the first error corresponds to variation of the CKM parameters, the second and third errors refer to uncertainties in the hadronic parameters used in the calculation and the fourth error reflects additional uncertainties caused by the breakdown of the factorization ansatz (that result in endpoint singularities regulated in terms of two extra complex parameters). Because

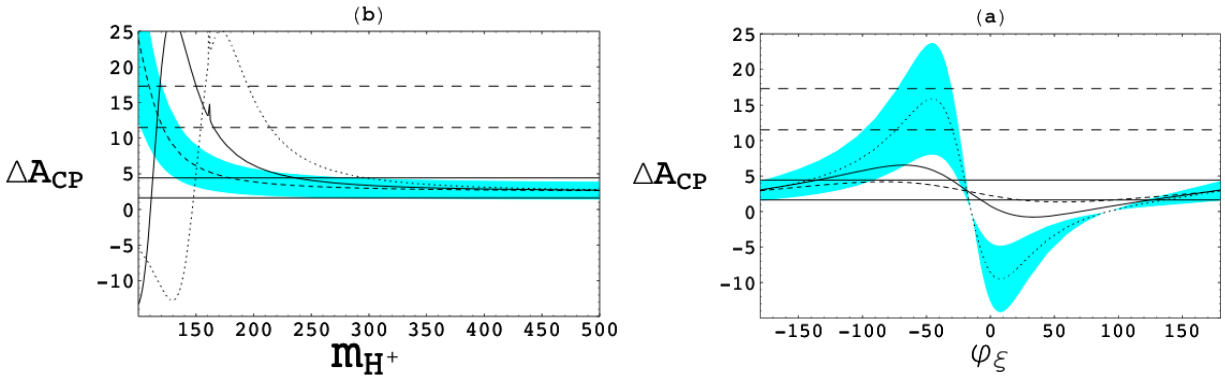

Figure 17: $m_{H^\pm}$ and φ_ξ dependence of the T2HDM contributions to ΔA_{CP}. Solid, dashed and dotted lines correspond to $(\tan\beta_H, |\xi|) = (50,1)$, $(35,1)$ and $(50,2)$, respectively. The blue band is the experimental 68% C.L. allowed region. In plot (a) and (b) we fix $\varphi_\xi = -50^o$ and $m_{H^\pm} = 200$ GeV, respectively.

of a high degree of correlation, most of these errors cancel when considering the difference between these two asymmetries. From Ref. [31], we see that this difference lies in the range $[0.5, 3.3]$. Using the formulae presented in Ref. [98] and updated numerical inputs, we find

$$\Delta A_{CP} \equiv A_{CP}(B^- \to K^-\pi^0) - A_{CP}(\bar{B}^0 \to K^-\pi^+) = 2.1(1 \pm 0.5)\ , \tag{131}$$

where the 50% error reflects the uncertainties studied in Ref. [31] and the possibility unusually large power corrections (scenarios S1–S4 of Ref. [31]). This SM estimate has to be compared to the present experimental results [14]:

$$A_{CP}(B^- \to K^-\pi^0) = (4.7 \pm 2.6)\,\% \tag{132}$$

$$A_{CP}(\bar{B}^0 \to K^-\pi^+) = (-9.7 \pm 1.2)\,\% \tag{133}$$

$$\Delta A_{CP} = (14.4 \pm 2.9)\,\%\ . \tag{134}$$

The effective Hamiltonian responsible for T2HDM contributions to ΔA_{CP} and the relevant matching conditions have been given in Sec. 5.4. For completeness we point out that other approaches to the calculation of ΔA_{CP} (see, for instance, Ref. [99]) are consistent with the QCD-factorization results. Also note that it might be possible to accommodate the present experimental results in models in which the color–suppressed tree contribution is unusually enhanced [100].

In Fig. 17 we show the size of T2HDM contributions to ΔA_{CP}. Unfortunately, for $m_{H^\pm}$ larger than 300 GeV we do not find any sizable effect.

6 Observables: the neutral Higgs sector

6.1 $(g-2)_\mu$

The anomalous magnetic moment of the muon receive potentially large contributions at the 2–loop level via the Barr–Zee mechanism [101,102]. These diagrams are able to account for the large discrepancy between the SM prediction and the experimental measurement only for very light pseudo–scalar mass ($m_A < 100$ GeV) [103].

6.2 $\Delta\rho$

T2HDM contributions to $\Delta\rho$ depend on both the neutral and charged Higgs bosons. For any choice of the charged Higgs mass it is possible to find region of the (m_A, m_H and α_H) parameter space for which the corrections to the ρ–parameter are in agreement with the experimental bounds.

6.3 $Z \to b\bar{b}$

Charged and neutral Higgs contributions to the effective $Z-b-\bar{b}$ coupling affect both the ratio $R_b \equiv \Gamma(Z \to b\bar{b})/\Gamma(Z \to \text{hadrons})$ and the forward–backward asymmetry A_b. The present experimental results are [25]:

$$R_b = 0.21629 \pm 0.00066 \tag{135}$$

$$A_b = 0.901 \pm 0.013\ , \tag{136}$$

where the value for A_b has been obtained by combining the direct and indirect measurements (from $A_b = 4/3\ A_{\rm fb}^{0,b}/A_\ell$). The SM fits for these two observables read: $R_b^{SM} = 0.21586$ and $A_b^{SM} = 0.935$. In particular note that A_b shows a deviation of about 2.5σ from the SM prediction.

The T2HDM contribution to the effective $Z \to b\bar{b}$ vertex can be easily extracted from the results of Ref. [104]. These corrections depend on both the charged and neutral Higgs sector of the T2HDM. Unfortunately we do not find any sizable effect in the portion of the parameter space allowed by the other constraints.

7 Summary & Outlook

Thanks to the spectacular performance of the two asymmetric B-factories, intensive studies in the last few years have demonstrated that the CP and flavor violation observed in B and K physics is described by the standard CKM mechanism to an accuracy of about 15%. A very interesting result, potentially one of the most important discovery made at the B-factories, is that the time dependent CP-asymmetries in penguin dominated modes do not seem to agree with the SM expectations. At the moment these deviations are in the 2.5-3.5σ ranges. Since

these modes are short-distance dominated, they are very sensitive to presence of beyond the Standard Model phases. Taking seriously this pieces of data is suggestive of sizable contributions from a non-standard phase. For the sake of completeness we also mentioned several other measurements that display a significant deviation from the SM, such as difference in the CP asymmetry between $K^+\pi^-$ and $K^+\pi^0$, the (g-2) of the muon and the forward-backward asymmetry in $Z \to b\bar{b}$ measured at LEP

As an illustration of a new physics scenario that may account for the observed deviations from the SM we have presented a detailed study of the two Higgs doublet model for the top quark. The model is a simple extension of the SM which in a natural way accounts for the very heavy top mass. We view it as an interesting low energy effective model that encompasses some of the important features of an underlying framework of dynamical electroweak symmetry breaking. Of course, the deviations seen in B decays and other flavor physics, may also be accountable by many other extensions of the SM; for example supersymmetry [10], a fourth family [11], a Z-penguin [12] or warped flavor-dynamics [13]. Obviously, the main features of any extension of the Standard Model that is to account for the experimental deviations in B-physics and other flavor physics that are discussed here are that there have to be new particles in the $\approx$ 300 GeV to $\approx$ few TeV range and associated with these one needs at least one new CP-odd phase. Distinguishing between various scenarios or nailing down the precise structure of some other models responsible for the deviations that we have discussed will undoubtedly require much more experimental information. In any case if the hints from the B-factories are really true, we will certainly witness a truly exciting era in Particle Physics as the LHC starts its long awaited operations in 2008. It should also be abundantly clear that infusion of precise information from low energy flavor measurements will be crucial in interpreting the findings at the terascale energy.

Acknowledgments

This research was supported in part by the U.S. DOE contract No.DE-AC02-98CH10886(BNL). Research partly supported by the Department of Energy under Grant DE-AC02-76CH030000. Fermilab is operated by Fermi Research Alliance, LLC under Contract No. DE-AC02-07CH11359 with the United States Department of Energy.

References

[1] See, *e.g.* the talk by Masashi Hazumi at the International Conference on High Energy Physics, 2006 (Moscow, Russia)

[2] N. Cabibbo, Phys. Rev. Lett. **10** (,) 531 (1963); M. Kobayashi and T. Maskawa, Prog. Theor. Phys. **49** (,) 652 (1973)

[3] A. G. Akeroyd *et al.* [SuperKEKB Physics Working Group], arXiv:hep-ex/0406071.

[4] J. L. Hewett *et al.*, arXiv:hep-ph/0503261.

[5] J. Albert *et al.*, arXiv:physics/0512235.

[6] A. K. Das and C. Kao, Phys. Lett. B **372**, 106 (1996) [arXiv:hep-ph/9511329].

[7] K. Kiers, A. Soni and G. H. Wu, Phys. Rev. D **59**, 096001 (1999) [arXiv:hep-ph/9810552].

[8] G. H. Wu and A. Soni, Phys. Rev. D **62**, 056005 (2000) [arXiv:hep-ph/9911419].

[9] See also: M. Neubert talk at the Electrowek Session of Moriond 2007.

[10] See, *e.g.* L. Silvestrini, hep-ph/07051624 and references therein.

[11] W.-S. Hou, H.-n Li, S. Mishima and M. Nagashima, Phys. Rev. Lett. 98, 131801 (2007).

[12] David Atwood and G. Hiller, hep-ph/0307251.

[13] K. Agashe, G. Perez and A. Soni, hep-ph/0406101; hep-ph/0408134; K. Agashe, M. Papucci, G. Perez and D. Pirjol, hep-ph/0509117.

[14] E. Barberio *et al.* [Heavy Flavor Averaging Group (HFAG)], arXiv:hep-ex/0603003.

[15] D. J. Antonio *et a.* [RBC Collaboration], arXiv:hep-ph/0702042.

[16] Note that our fit results are completely compatible with the UTfit ($\sin 2\beta = 0.759 \pm 0.037$), see M. Bona *et al*, hep-ph/0606167. It is also consistent with the CKMfitter group ($\sin 2\beta = 0.823^{+0.018}_{-0.085}$), see J. Charles *et al* hep-ph/0406184. Note, in particular, that while the latter's errors with the negative sign are somewhat bigger compared to ours their central value is appreciably bigger so that the devaitions that are of concern to us remain essentially unaffected.

[17] Y. Grossman and M. Worah, Phys. Lett. **B395**, 241(1997);

[18] Y. Grossman, G. Isidori and M. P. Worah, Phys. Rev. D **58**, 057504 (1998) [arXiv:hep-ph/9708305].

[19] D. London and A. Soni, Phys. Lett. **B401**, 61 (1997).

[20] H.-Y Cheng, C.-K Chua and A. Soni, Phys. Rev. **D72**, 014006 (2005); Phys. Rev. **D 72**, 094003 (2005).

[21] M. Beneke, Phys. Lett. B **620**, 143 (2005) [arXiv:hep-ph/0505075].

[22] G. Buchalla, G. Hiller, Y. Nir and G. Raz, JHEP **0509**, 074 (2005).

[23] A. Williamson and J. Zupan, Phys. Rev. **D74**, 014003 (2006); hep-ph/0601214.

[24] T. Gershon and M. Hazumi, Phys. Lett. **B596**, 163(2004).

[25] W. M. Yao *et al.* [Particle Data Group], J. Phys. G **33**, 1 (2006).

[26] H. G. Evans [CDF Collaboration], arXiv:0705.4598 [hep-ex].

[27] M. Bona *et al.* [UTfit Collaboration], arXiv:hep-ph/0606167.

[28] See also: C. Dawson PoS LAT2005:007,2006.

[29] P. B. Mackenzie, eConf **C060409**, 022 (2006) [arXiv:hep-ph/0606034].

[30] M. Beneke, G. Buchalla, M. Neubert and C. T. Sachrajda, Nucl. Phys. B **591**, 313 (2000) [arXiv:hep-ph/0006124].

[31] M. Beneke and M. Neubert, Nucl. Phys. B **675**, 333 (2003) [arXiv:hep-ph/0308039].

[32] M. Passera, arXiv:hep-ph/0702027.

[33] J. P. Miller, E. de Rafael and B. L. Roberts, Rept. Prog. Phys. **70**, 795 (2007) [arXiv:hep-ph/0703049].

[34] G. W. Bennett *et al.* [Muon g-2 Collaboration], Phys. Rev. Lett. **92**, 161802 (2004) [arXiv:hep-ex/0401008].

[35] G. W. Bennett *et al.* [Muon G-2 Collaboration], Phys. Rev. D **73**, 072003 (2006) [arXiv:hep-ex/0602035].

[36] Z. j. Xiao and L. x. Lu, arXiv:hep-ph/0605076.

[37] W. A. Bardeen, C. T. Hill and M. Lindner, Phys. Rev. D **41**, 1647 (1990).

[38] V. A. Miransky, M. Tanabashi and K. Yamawaki, Phys. Lett. B **221**, 177 (1989).

[39] C. T. Hill, Phys. Lett. B **266**, 419 (1991).

[40] G. Buchalla, G. Burdman, C. T. Hill and D. Kominis, Phys. Rev. D **53**, 5185 (1996) [arXiv:hep-ph/9510376].

[41] T. P. Cheng and M. Sher, Phys. Rev. D **35**, 3484 (1987).

[42] CLEO Collaboration (S. Chen *et al.*), Phys. Rev. Lett. **87**, 251807 (2001).

[43] Belle Collaboration (K. Abe *et al.*), Phys. Lett/ B **511**, 151 (2001).

[44] Belle Collaboration (P. Koppunberg *et al.*), Phys. Rev. Lett. **93**, 061803 (2004).

[45] BaBar Collaboration (B. Aubert *et al.*), Phys. Rev. D **72**, 052004 (2005).

[46] BaBar Collaboration (B. Aubert *et al.*), hep-ex/0507001.

[47] Heavy Flavor Averaging Group, arXiv:hep-ex/0603003.

[48] M. Iwasaki *et al.* [Belle Collaboration], hep-ex/0503044.

[49] B. Aubert *et al.* [BABAR Collaboration], Phys. Rev. Lett. **93** (2004) 081802 [hep-ex/0404006].

[50] T. Huber, E. Lunghi, M. Misiak and D. Wyler, Nucl. Phys. B **740**, 105 (2006) [arXiv:hep-ph/0512066].

[51] K. Kiers, A. Soni and G. H. Wu, Phys. Rev. D **62**, 116004 (2000) [arXiv:hep-ph/0006280].

[52] T. Hurth, E. Lunghi and W. Porod, Nucl. Phys. B **704**, 56 (2005) [arXiv:hep-ph/0312260].

[53] E. Lunghi and J. Matias, JHEP **0704**, 058 (2007) [arXiv:hep-ph/0612166].

[54] M. Misiak *et al.*, arXiv:hep-ph/0609232.

[55] M. Misiak and M. Steinhauser, arXiv:hep-ph/0609241.

[56] S. J. Lee, M. Neubert and G. Paz, arXiv:hep-ph/0609224.

[57] T. Becher and M. Neubert, arXiv:hep-ph/0610067.

[58] A. H. Hoang and A. V. Manohar, hep-ph/0509195.

[59] [CDF Collaboration], hep-ex/0507091.

[60] S. Bethke, Nucl. Phys. Proc. Suppl. **135**, 345 (2004) [arXiv:hep-ex/0407021].

[61] C. W. Bauer, Z. Ligeti, M. Luke, A. V. Manohar and M. Trott, Phys. Rev. D **70**, 094017 (2004) [arXiv:hep-ph/0408002].

[62] A. J. Buras, P. H. Chankowski, J. Rosiek and L. Slawianowska, Nucl. Phys. B **619**, 434 (2001) [arXiv:hep-ph/0107048].

[63] M. Battaglia *et al.*, arXiv:hep-ph/0304132.

[64] A. J. Buras, arXiv:hep-ph/9806471.

[65] A. J. Buras, S. Jager and J. Urban, Nucl. Phys. B **605**, 600 (2001) [arXiv:hep-ph/0102316].

[66] E. Dalgic *et al.*, arXiv:hep-lat/0610104.

[67] C. Aubin *et al.* [MILC Collaboration], Phys. Rev. D **70**, 114501 (2004) [arXiv:hep-lat/0407028].

[68] A. A. Petrov, Phys. Rev. D **56**, 1685 (1997) [arXiv:hep-ph/9703335].

[69] R. Gupta, T. Bhattacharya and S. R. Sharpe, Phys. Rev. D **55**, 4036 (1997) [arXiv:hep-lat/9611023].

[70] H. W. Lin, S. Ohta, A. Soni and N. Yamada, Phys. Rev. D **74**, 114506 (2006) [arXiv:hep-lat/0607035].

[71] A. J. Buras, P. H. Chankowski, J. Rosiek and L. Slawianowska, Nucl. Phys. B **659**, 3 (2003) [arXiv:hep-ph/0210145].

[72] J. Bijnens, J. M. Gerard and G. Klein, Phys. Lett. B **257**, 191 (1991).

[73] D. Becirevic, V. Gimenez, G. Martinelli, M. Papinutto and J. Reyes, JHEP **0204**, 025 (2002) [arXiv:hep-lat/0110091].

[74] D. Becirevic, V. Gimenez, G. Martinelli, M. Papinutto and J. Reyes, Nucl. Phys. Proc. Suppl. **106**, 385 (2002) [arXiv:hep-lat/0110117].

[75] P. Ball and R. Fleischer, Eur. Phys. J. C **48**, 413 (2006) [arXiv:hep-ph/0604249].

[76] E. Golowich and A. A. Petrov, Phys. Lett. B **625**, 53 (2005) [arXiv:hep-ph/0506185].

[77] E. Golowich, J. Hewett, S. Pakvasa and A. A. Petrov, arXiv:0705.3650 [hep-ph].

[78] B. Aubert [BABAR Collaboration], arXiv:hep-ex/0703020.

[79] K. Abe [Belle Collaboration], arXiv:hep-ex/0703036.

[80] M. Ciuchini, E. Franco, D. Guadagnoli, V. Lubicz, M. Pierini, V. Porretti and L. Silvestrini, arXiv:hep-ph/0703204.

[81] K. Ikado *et al.*, arXiv:hep-ex/0604018.

[82] B. Aubert [BABAR Collaboration], arXiv:hep-ex/0608019.

[83] E. Gabrielli and G. F. Giudice, Nucl. Phys. B **433**, 3 (1995) [Erratum-ibid. B **507**, 549 (1997)] [arXiv:hep-lat/9407029].

[84] H. Y. Cheng and K. C. Yang, Phys. Rev. D **63**, 074011 (2001) [arXiv:hep-ph/0011179].

[85] E. Gabrielli, K. Huitu and S. Khalil, Nucl. Phys. B **710**, 139 (2005) [arXiv:hep-ph/0407291].

[86] M. Ciuchini, E. Franco, V. Lubicz, F. Mescia and C. Tarantino, JHEP **0308**, 031 (2003) [arXiv:hep-ph/0308029].

[87] A. Lenz, arXiv:hep-ph/0412007.

[88] A. Lenz and U. Nierste, arXiv:hep-ph/0612167.

[89] V. M. Abazov [D0 Collaboration], arXiv:hep-ex/0701012.

[90] M. Beneke, G. Buchalla, A. Lenz and U. Nierste, Phys. Lett. B **576**, 173 (2003) [arXiv:hep-ph/0307344].

[91] D. E. Jaffe *et al.* [CLEO Collaboration], Phys. Rev. Lett. **86**, 5000 (2001) [arXiv:hep-ex/0101006].

[92] E. Nakano *et al.* [Belle Collaboration], Phys. Rev. D **73**, 112002 (2006) [arXiv:hep-ex/0505017].

[93] B. Aubert *et al.* [BABAR Collaboration], Phys. Rev. Lett. **96**, 251802 (2006) [arXiv:hep-ex/0603053].

[94] M. Kuze [H1 collaboration], arXiv:hep-ex/9910017.

[95] R. Barate *et al.* [ALEPH Collaboration], Eur. Phys. J. C **20**, 431 (2001).

[96] Y. Grossman, Y. Nir and G. Raz, Phys. Rev. Lett. **97**, 151801 (2006) [arXiv:hep-ph/0605028].

[97] T. Ibrahim and P. Nath, Phys. Rev. D **57**, 478 (1998) [Erratum-ibid. D **58**, 019901 (1998 ERRAT,D60,079903.1999 ERRAT,D60,119901.1999)] [arXiv:hep-ph/9708456].

[98] S. Khalil, Phys. Rev. D **72**, 035007 (2005) [arXiv:hep-ph/0505151].

[99] H. Y. Cheng, C. K. Chua and A. Soni, Phys. Rev. D **71**, 014030 (2005) [arXiv:hep-ph/0409317].

[100] M. Gronau and J. L. Rosner, Phys. Rev. D **74**, 057503 (2006) [arXiv:hep-ph/0608040].

[101] J. D. Bjorken and S. Weinberg, Phys. Rev. Lett. **38**, 622 (1977).

[102] S. M. Barr, E. M. Freire and A. Zee, Phys. Rev. Lett. **65**, 2626 (1990).

[103] K. Cheung and O. C. W. Kong, Phys. Rev. D **68**, 053003 (2003) [arXiv:hep-ph/0302111].

[104] A. Denner, R. J. Guth, W. Hollik and J. H. Kuhn, Z. Phys. C **51**, 695 (1991).

[105] See also, *e.g.*, W.-S. Hou, H.-n Li, S. Mishima and M. Nagashima, Phys. Rev. Lett. 98, 131801 (2007); M. Neubert talk at the Electrowek Session of Moriond 2007.